Supplementary Information (SI) for Physical Chemistry Chemical Physics.
This journal is © the Owner Societies 2024

Electronic Supplementary Information

Engineering High-Brightness and Long-Lived Organic Room-Temperature Phosphorescence via Systematic Molecular Design

Guangming Wang,[#a] Yuanyuan Chen,[#a,b] Xuefeng Chen,[#a] Jinqi Zha,*[c], Xiaoya Guo*[b] and Kaka Zhang*[a]

[a] State Key Laboratory of Organometallic Chemistry and Shanghai-Hong Kong Joint Laboratory in Chemical Synthesis, Key Laboratory of Synthetic and Self-Assembly Chemistry for Organic Functional Molecules, Ningbo Zhongke Creation Center of New Materials, Shanghai Institute of Organic Chemistry, University of Chinese Academy of Sciences, Chinese Academy of Sciences, 345 Lingling Road, Shanghai 200032, People's Republic of China. E-mail: zhangkaka@sioc.ac.cn;

[b] Department of Chemical Engineering, Shanghai University, Shanghai, 200444, China. Email: gxy@shu.edu.cn;

[c] Ingenuity Biotechnology (Shanghai) Co., Ltd., 9th Floor, Block B, Building 1, No. 955 Liuxiang Road, Nanxiang Town, Jiading District, Shanghai 201802, People's Republic of China. E-mail: check.zha@ingenuitybio.com.

#equal contribution

Table of Contents

1 Experimental Procedures

1.1 Materials

Acetophenone (99%, Aladdin), 1'-acetonaphthone (95%, Innochem), 6-methoxy-2-acetonaphthone (98%, adamas), 2-acetonaphthone (98%, Bidepharm), 5'-bromo-1,1':3',1"-terphenyl (98%, Bidepharm), 2-methoxynaphthalene-1-boronic acid (98%, Innochem), palladium (II) acetate (98%, Shaoyuanchem), potassium carbonate (99%, Dahechem), acetic anhydride (98.5%, Sinopharm Chemical Reagent), boron trifluoride diethyl etherate (98%, TCI), phenyl benzoate (PhB) (99%, Energy Chemical).

1.2 Physical measurements and instrumentation

Nuclear magnetic resonance (NMR) spectra were recorded on a JEOL Fourier-transform NMR spectrometer (400 MHz), including ^{1}H NMR, ^{13}C NMR, ^{19}F NMR and ^{11}B NMR. Mass spectra were performed on Agilent Technologies 5973N and Thermo Fisher Scientific LTQ FT Ultras mass spectrometer. FT-IR spectra were recorded on a Nicolet AVATAR-360 FT-IR spectrophotomerter with a resolution of 4 cm^{-1}. X-Ray diffraction data of the crystals were collected using synchrotron radiation (λ = 0.82652 Å) on beamline 17 B at the National Facility for Protein Science Shanghai (NFPS) in the Shanghai Synchrotron Radiation Facility, People's Republic of China. The diffraction data reduction and integration were performed by the HKL3000 software. The structures were solved by direct methods and refined employing full-matrix least-squares on F2 by using SHELXL program through the OLEX2 interface (Sheldrick G, Crystal Structure Refinement with SHELXL. *Acta. Crystallogr. Sect. C* 2015, 71: 3-8; Dolomanov OV, Bourhis L J, Gildea R J, Howard JAK and Puschmann H, OLEX2: A Complete Structure Solution, Refinement and Analysis Program. *J. Appl. Crystallogr.* 2009, 42: 339-341). All non-H atoms of the compounds were refined with anisotropic thermal parameters. The hydrogen atoms were included in idealized positions and refined with fixed geometry with respect to their carrier atoms. Refinement data of the compounds was processed by using SQUEEZE program (Spek A, Single-crystal Structure Validation with the Program PLATON. *J. Appl. Crystallogr.* 2003, 36: 7-13). The X-ray crystallographic data for the compounds has been deposited at the Cambridge Crystallographic Data Centre (CCDC), under the deposition number CCDC 2226200 (compound **4**). UV-Vis absorption spectra were recorded on a Techcomp UV1050 UV-vis spectrophotometer. The steady-state and delayed emission spectra were collected by Hitachi FL-4700 fluorescence spectrometer equipped with chopping systems; the delayed emission spectra were obtained with a delay time of approximately 1 ms. The excited state decay profiles in millisecond to second region were collected by Hitachi FL-4700 fluorescence spectrometer equipped with chopping systems. Emission spectra were recorded using Edinburgh FLS1000 fluorescence spectrometer, Hitachi FL-7000 fluorescence spectrometer and Horiba FluoroLog-3 fluorescence spectrometer. The fluorescence decay profiles in nanosecond region were recorded by using time-correlated single photon counting technique (TCSPC) on a

Edinburgh FLS1000 fluorescence spectrometer equipped with a picosecond pulsed diode laser. Photoluminescence quantum yield was measured by a Hamamatsu absolute PL quantum yield measurement system based on a standard protocol (*Adv. Mater.* **1997**, *9*, 230). Photographs and videos were captured by HUAWEI P30 and iphone 12 cameras. Before the capture, samples were irradiated by a 365 nm UV lamp (5 W) for approximately 5 s at a distance of approximately 15 cm.

1.3 TD-DFT calculations

TD-DFT calculations were performed to study the photophysical properties of molecularly dispersed **BF_2bdk** in the solid state. Since the afterglow properties are originated from the excited states of molecularly dispersed **BF_2bdk** in the rigid PhB matrices where intermolecular rotation and vibration are largely restricted, the ground-state geometry of **BF_2bdk** was used for all the TD-DFT calculations. The ground-state geometry of compounds **1-4** were optimized by a DFT calculation using B3LYP functional and 6-31G (d, p) basis set. The singlet excited states and triplet excited states were calculated on ORCA 4.2.1 program with B3LYP functional and def2-TZVP(-f) basis set and analyzed by Multiwfn software. Spin-orbit coupling (SOC) matrix elements between the singlet excited states and triplet excited states were calculated with spin-orbit mean-field (SOMF) methods on ORCA 4.2.1 program with B3LYP functional and def2-TZVP(-f) basis set. The obtained electronic structures were analyzed by Multiwfn software. All iso-surface maps to show the electron distribution and electronic transitions were rendered by Visual Molecular Dynamics (VMD) software based on the exported files from Multiwfn. (Neese F, *Wiley Interdiscip. Rev. Comput. Mol. Sci.* 2018, 8: 1327-1332; Becke AD, *Phys. Rev. A* 1988, 38: 3098-3100; Lee C, Yang W, Parr RG, *Phys. Rev. B.* 1988, 37: 785-789; Miehlich B, Savin A, Stoll H, Preuss H, *Chem. Phys. Lett.* 1989, 157: 200-206; Roy LE, Hay PJ, Martin RL, *J. Chem. Theory Comput.* 2008, 4: 1029–1031; Weigend F, Ahlrichs R, *Phys. Chem. Chem. Phys.* 2005, 7: 3297-3305; Lu T, Chen F, *J. Comput. Chem.* 2012, 33: 580-592; Humphrey W, Dalke A, Schulten K, *J. Mol. Graphics* 1996, 14: 33-38).

1.4 Synthesis

Synthesis of compound 1

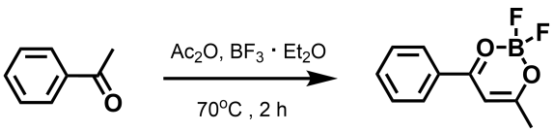

Synthesis of compound **1** was carried out following the previous literature (*Chem. Commun*., **2021**, *57*, 8794–8797). Into a round bottom flask was added 0.36 mL acetophenone (3.0 mmol), 4.00 mL acetic anhydride and 1.20 mL boron trifluoride diethyl etherate (9.5 mmol). The reaction mixture was heated to 70 °C for 2 h. After cooling to room temperature, the reaction mixture was

extracted with dichloromethane and washed with deionized water. The obtained crude product in dichloromethane was dried over anhydrous sodium sulphate, condensed by rotary evaporation, and then purified by column chromatography over silica gel using the petroleum ether/ dichloromethane (1/1, v/v) as eluent to give 520 mg pale yellow solids with an isolation yield of 82.5%. The compound **1** was further purified by three cycles of recrystallization in spectroscopic grade dichloromethane/hexane. ^{1}H NMR (400 MHz, Chloroform-*d*, 298 K, relative to Me_4Si /ppm) δ 8.09 – 8.04 (m, 2H), 7.73 – 7.66 (m, 1H), 7.54 (t, *J* = 7.9 Hz, 2H), 6.58 (s, 1H), 2.43 (s, 3H). ^{13}C NMR (101 MHz, Chloroform-*d*) δ 192.61, 182.93, 135.49, 131.20, 129.20, 129.03, 97.45, 24.80. ^{19}F NMR (376 MHz, Chloroform-*d*, 298 K, relative to $CFCl_3$ /ppm) δ -139.17, -139.23. ^{11}B NMR (128 MHz, Chloroform-*d*, 298 K, relative to $BF_3{\cdot}OEt_2$ /ppm) δ 0.05. LRMS, m/z 209. HRMS (positive EI) m/z found (calcd for $C_{10}H_9O_2{}^{10}BF_2$): 209.0690 (209.0694).

Synthesis of compound 2

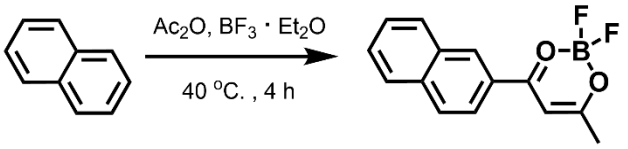

Synthesis of compound **2** was carried out following the previous literature (*Chin. J. Chem.* **2024**, *42*, 1237-1246). Into a round bottom flask were added 2-acetonaphthone (170 mg, 1.0 mmol), acetic anhydride (5 mL) and boron trifluoride diethyl etherate (0.4 mL). The reaction mixture was stirred at 40 °C for 4 h. After cooling to room temperature, the reaction was quenched by adding the reaction mixture dropwise into cold water. The precipitates were washed by water for three times and dried under vacuum. The crude product was purified by column chromatography over silica gel using petroleum ether/dichloromethane (1:1) as eluent to give yellow solids (224 mg, yield 86%). The obtained **2** was further purified by three cycles of recrystallization in spectroscopic grade dichloromethane/hexane. ^{1}H NMR (400 MHz, chloroform-*d*) δ: 8.70 (s, 1H), 7.99 (dd, J = 8.7, 1.7 Hz, 2H), 7.94 (d, J = 8.7 Hz, 1H), 7.90 (d, J = 8.1 Hz, 1H), 7.71—7.65 (m, 1H), 7.63—7.58 (m, 1H), 6.72 (s, 1H), 2.46 (s, 3H). ^{19}F NMR (376 MHz, Chloroform-*d*) δ: –138.74, –138.80. ^{13}C NMR (101 MHz, DMSO-d_6) δ: 194.09, 181.10, 136.15, 132.19, 131.79, 130.13, 130.08, 129.19, 127.94, 127.90, 127.63, 123.50, 98.62, 24.54. ^{11}B NMR (128 MHz, DMSO-d_6) δ: 0.03. HRMS (positive): measured for [$C_{14}H_{11}BF_2O_2$ + Na^+] 283.0718, calculated 283.0715.

Synthesis of compound 3

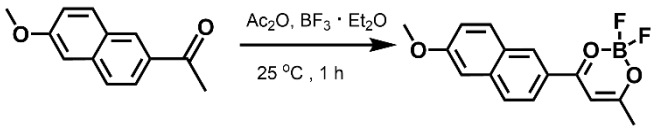

Into a round bottom flask were 6-methoxy-2-acetonaphthone (200.0 mg, 1 mmol), acetic anhydride (2.0 mL, 21.6 mmol) and boron trifluoride diethyl etherate (0.65 mL, 5.24 mmol). The

reaction mixture was kept at 25°C and stirred for 1 h. Then the reaction was quenched by adding the reaction mixture dropwise into cold water. The crude product was extracted with dichloromethane and washed with deionized water. The obtained crude product in dichloromethane was dried over anhydrous Na_2SO_4, condensed by rotary evaporation, and then purified by column chromatography over silica gel using petroleum ether/dichloromethane (2:1) as eluent to give yellow solid compound **3**. The compound **3** was further purified by three cycles of recrystallization in spectroscopic grade dichloromethane /hexane. ^{1}H NMR (400 MHz, DMSO-d_6, relative to Me_4Si /ppm) δ 8.84 (d, J = 2.1 Hz, 1H), 8.09 (d, J = 9.1 Hz, 2H), 7.98 (s, 1H), 7.45 (s, 1H), 7.30 (d, J = 8.8 Hz, 2H), 3.92 (s, 3H), 2.48 (s, 3H). ^{13}C NMR (126 MHz, DMSO-d_6) δ 193.10, 181.61, 161.17, 138.88, 132.38, 132.27, 128.32, 128.05, 125.83, 124.71, 120.74, 106.82, 98.43, 56.12, 24.81. ^{19}F NMR (376 MHz, DMSO-d6) δ -123.00, -123.06. ^{11}B NMR (128 MHz, DMSO-d_6) δ 0.02. HRMS (positive): measured for [$C_{15}H_{13}BF_2O_3$ + NH_4^+] 307.1300, calculated 307.1300.

Synthesis of compound 4

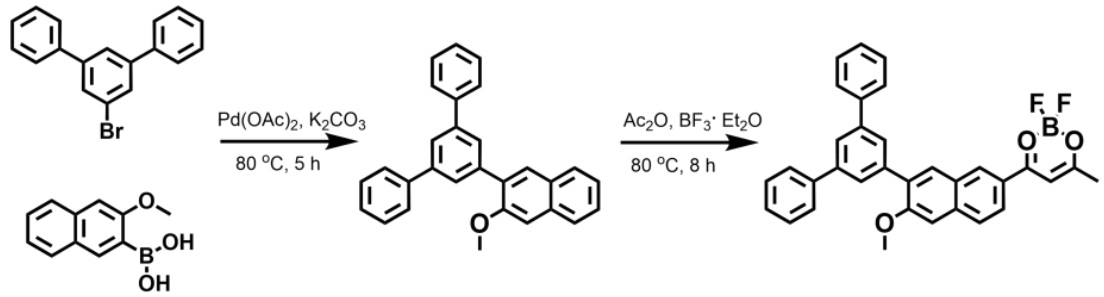

Into a round bottom flask were 5'-bromo-1,1':3',1"-terphenyl (309.2 mg, 1.0 mmol), 2-methoxynaphthalene-1-boronic acid (238.4 mg, 1.18 mmol), K_2CO_3 (138.4 mg, 1.0 mmol), Pd $(OAc)_2$ (11.1 mg, 0.05 mmol), ethanol (10 mL) and deionized water (1mL). The reaction mixture was heated to 80 °C and stirred for 5 h. After cooling to room temperature, the reaction mixture was diluted by dichloromethane, and K_2CO_3 precipitates were removed by suction filtration. The obtained crude product was condensed by rotary evaporation, and then purified by column chromatography over silica gel using petroleum ether/dichloromethane (3:1) as eluent to give colorless transparent oil. The colorless transparent oil was then added to a round bottom flask containing acetic anhydride (1.5 mL) and boron trifluoride diethyl etherate (0.8 mL). The reaction mixture was stirred for 8 hours at 80 °C. The reaction mixture was extracted with dichloromethane and washed with deionized water. The crude product was dried on anhydrous magnesium sulfate, concentrated by rotary evaporation. The crude product purified by column chromatography over silica gel using petroleum ether/dichloromethane (1:2) to give pale yellow compound **4**. The compound **4** was further purified by three cycles of recrystallization in spectroscopic grade dichloromethane/hexane (CCDC 2226200). ^{1}H NMR (400 MHz, Chloroform-*d*， relative to Me_4Si /ppm) δ 8.66 (d, J = 1.6 Hz, 1H), 8.03 (m, 2H), 7.87 (d, J = 14.3 Hz, 2H), 7.80 (d, J = 1.6 Hz, 2H),

7.71 (d, J = 7.3 Hz, 4H), 7.48 (d, J = 7.6 Hz, 4H), 7.40 (t, J = 7.4 Hz, 2H), 7.31 (s, 1H), 6.68 (s, 1H), 4.03 (s, 3H), 2.44 (s, 3H). ^{19}F NMR (376 MHz, Chloroform-d) δ -139.14, -139.20. FT-IR: (KBr, cm^{-1}): ν 3039.3, 1620.8, 1593.2, 1530.1, 1477.5, 1460.1, 1432.5, 1415.5, 1383.5, 1369.9, 1339.3, 1315.4, 1259.8, 1241.8, 1195.1, 1164.8, 1151.0, 1103.2, 1079.6, 1053.1, 1019.8, 930.6, 913.6, 875.8, 859.6, 796.6, 766.1, 713.3, 702.1, 626.3, 559.3, 541.9, 479.3. Because of its low solubility in common organic solvents, we didn't obtain satisfactory ^{13}C NMR spectrum for compound **4**. HRMS (positive): measured for [$C_{33}H_{25}BF_2O_3$ + Na^+] 541.1762, calculated 541.1763.

1.5 Preparation

Preparation of BF_2bdk-PhB samples

For the preparation of 0.01%-**1**-PhB sample, 10 μL compound **1** in dichloromethane (1 mg/mL) and 100 mg phenyl benzoate (PhB) were added into a 3 mL sample bottle, and the mixture was heated to 80 °C. After freezing under liquid nitrogen and standing at room temperature for tens of minutes, 0.01%-**1**-PhB sample was obtained. Other samples using different **BF_2bdk** molecules were prepared through the similar processes.

2 Results and Discussion

Text S1. The selection guidance of organic matrix

PhB matrix has a melting point of approximately 70°C and is in crystalline state at room temperature. The crystalline structure of PhB matrix can suppress nonradiative decay of luminescent dopants' triplet excited states within the matrix and can also inhibit oxygen diffusion to protect luminescent dopants' triplets from oxygen quenching. PhB matrix can disperse luminescent dopants and prevent afterglow quenching caused by the electronic coupling of BF_2bdk aggregates. Besides, PhB, which has a ground-state dipole moment of 1.94 D, can interact with BF_2bdk's S_1 excited state via dipole-dipole interaction (with less influence on BF_2bdk's T_1 energy levels), lower BF_2bdk's S_1 energy levels and thus narrow singlet-triplet splitting energy (ΔE_{ST}) to enhance intersystem crossing (*Nat. Commun.*, **2023,** *14*, 1987; *Adv. Opt. Mater.*, **2022**, *10*, 2101909). PhB don't have electronic absorption in UVA region (Figure S15) and its fluorescence and phosphorescence are insignificant, which show negligible influence on BF_2bdk's absorption and emission spectra. PhB has high T_1 energy levels of around 3.5 eV by TD-DFT calculation, which can minimize possible afterglow quenching caused by BF_2bdk-to-PhB energy transfer (*Sci. China Chem.,* **2023***, 66, 1120; Dyes Pig.*, **2023**, *210*, 110984).

Text S2. About the discussion on the RTP mechanism of BF_2bdk-PhB materials

We assign the room-temperature afterglow property of 0.01%-**BF_2bdk**-PhB materials to RTP-type organic afterglow by our previous work (*Chem. Commun.*, **2021**, *57*, 8794; *Adv. Optical Mater.* **2021**, *9*, 2100353; *ACS Appl. Mater. Interfaces* **2022**, *14*, 1587; *Chin. J. Chem.* **2024**, *42*, 1237), as well as a series of experimental observations and analyses. (1) The afterglow color of 0.01%-**BF_2bdk**-PhB materials after ceasing UV light at room temperature is significantly red-shifted compared to their fluorescence color under UV excitation (Figure 1A and 1B), as are their delayed emission spectra to their steady-state emission spectra at room temperature (Figure 1C and 1D). (2) The delayed emission spectra of 0.01%-**BF_2bdk**-PhB materials (take **1**-PhB and **4**-PhB for example) at 77 K display a similar phosphorescence maximum emission to that at room temperature (Figure S9 and S10). (3) The absence of triplet-to-singlet excited state energy transfer, the absence of donor-acceptor afterglow mechanism based on intermolecular charge transfer and retarded charge recombination, and the absence of afterglow mechanism caused by impurity (Text S2). (4) Theoretical calculation of **BF_2bdk** molecules support their potential to undergo efficient ISC process and phosphorescence emission (Figure S4 - S7), as well as their nice agreement with the experimental results.

Text S3. Ruling out other possible mechanism in BF_2bdk-PhB afterglow system.

Excited state energy transfer from RTP donors to luminescent acceptors has been reported to give rise to organic afterglow at room temperature (*Nat. Commun.* **2020**, *11*, 4802; *Angew. Chem. Int. Ed.* **2020**, *59*, 9393). The excited state energy transfer only occurs when the donors are sufficiently excited. In the present study, the afterglow emission of **BF_2bdk**-PhB-0.01% samples can be excited by 365 nm UV. Since PhB matrices possess negligible UV-vis no absorption at 365 nm (Figure 1B), the possibility of excited state energy transfer from PhB matrices to **BF_2bdk** for the emergence of room-temperature afterglow can be ruled out.

In some reported organic systems (*Nature* **2017**, *550*, 384), the donor-acceptor mechanism

possess charge-separated states within the organic materials. The retarded charge recombination in the rigid solid medium is responsible for the long persistent luminescence in organic systems. Intermolecular charge transfer in donor-acceptor systems can lead to the formation of charge-separated states, which is a prerequisite for the organic long persistent luminescence properties in donor-acceptor afterglow systems. In the present study, since the organic matrices such as PhB possess low-lying HOMOs and high-lying LUMOs when compared to **BF_2bdk** dopants, intermolecular charge transfer between dopants and matrices would be insignificant in the present system and thus the organic long persistent luminescence mechanism can be ruled out.

It has been reported recently that isomeric impurity is responsible for the emergence of organic room-temperature afterglow in carbazole systems (*Nat. Mater.* **2021**, 20, 175). In the present study, **BF_2bdk** powders show no afterglow properties at room temperature. The **BF_2bdk** compounds were purified by careful column chromatography followed by recrystallization in spectroscopic grade dichloromethane/*n*-hexane for three times. HPLC measurement confirms its high purity (Figure S2). The excitation spectra of **BF_2bdk**-PhB samples have been found to agree well with the BF_2bdk absorption, which further support that the afterglow property originates from BF_2bdk rather than impurity (Figure S16). Upon doping into PhB matrices, 0.01%-**BF_2bdk**-PhB samples exhibited significant afterglow properties under ambient conditions. When dispersed in organic matrices at low doping concentration such as 0.01 wt%, the **BF_2bdk** molecules and the possible impurities should be separated by organic matrices, so charge separation and recombination processes between **BF_2bdk** molecules and the possible impurities are statistically negligible. These experiments and analysis can rule out the possibility that the room-temperature afterglow of 0.01%-**BF_2bdk**-PhB materials is originated from some impurities.

Recent studies in the literature showed that triplet excited states of organic matrices with energy levels sandwiched between S_1 and T_1 states of phosphorescence dopants can mediate singlet-to-triplet ISC of the phosphorescence dopants, leading to the emergence of room-temperature afterglow (*Angew. Chem. Int. Ed.* **2020**, *59*, 16054). This mediation of ISC is not the case in the present **BF_2bdk**-PhB system because T_1 level of PhB matrices is much higher than both the S_1 and T_1 states of **BF_2bdk** molecules. Actually, according to the studies by Adachi's group and us, high T_1 levels of organic matrices are very important for the fabrication of high-performance afterglow materials since it can avoid afterglow quenching caused by triplet-to-triplet energy transfer from luminescent dopants to organic matrices (*Adv. Funct. Mater.* **2013**, *23*, 3386; *Angew. Chem. Int. Ed.* **2021**, *60*, 17138).

3 Figures and Tables

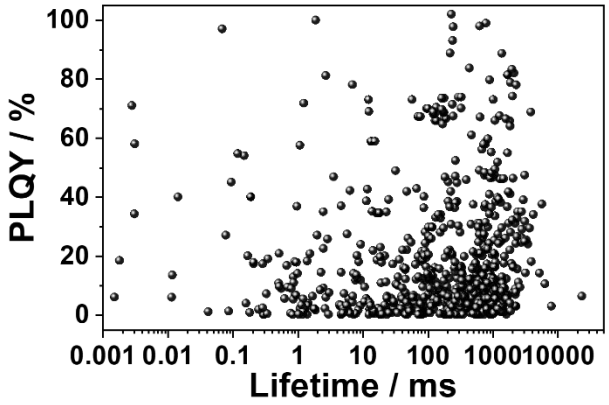

Figure S1. Photoluminescence quantum yields (PLQY) and afterglow emission lifetimes (τ) of organic RTP and afterglow materials in the previously reported studies.

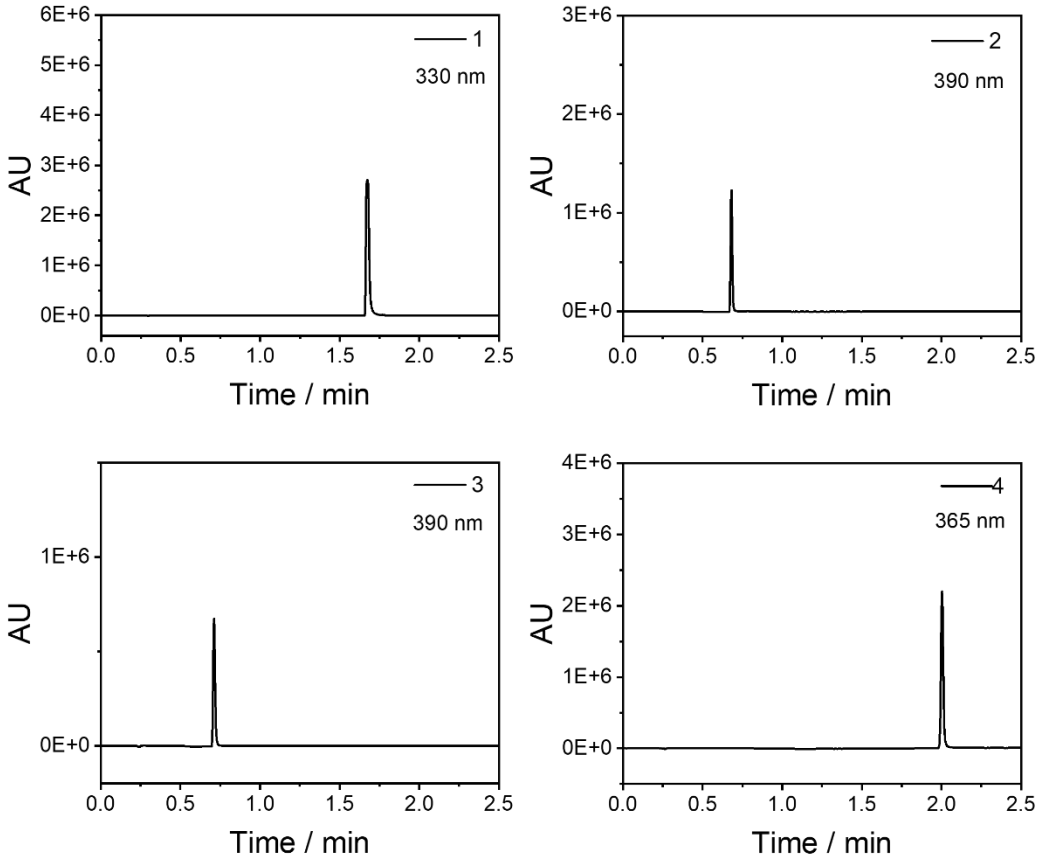

Figure S2. HPLC profiles of **BF_2bdk** molecules.

Table S1. Photophysical properties of **BF_2bdk** compounds in different solutions.

Compound	solvent	λ_{abs} / nm	$\varepsilon * 10^4$ / M^{-1} cm^{-1}	λ_{em} / nm	PLQY / %
1	DCM	330	3.18	3.18	3.18
	EA	329	2.75	373	0.534
	ACE	333	3.23	377	1.03
	THF	330	2.19	379	0.462
2	DCM	343	4.34	457	62.79
	EA	341	5.77	443	30.99
	ACE	340	4.91	442	33.42
	THF	342	8.74	464	24.75
3	DCM	387	2.69	470	13.73
	EA	381	4.87	461	39.37
	ACE	382	6.00	476	2.28
	THF	382	11.05	465	31.07
4	DCM	380	4.07	462	48.46
	EA	374	1.72	453	69.14
	ACE	377	4.30	473	65.45
	THF	376	3.99	454	70.14

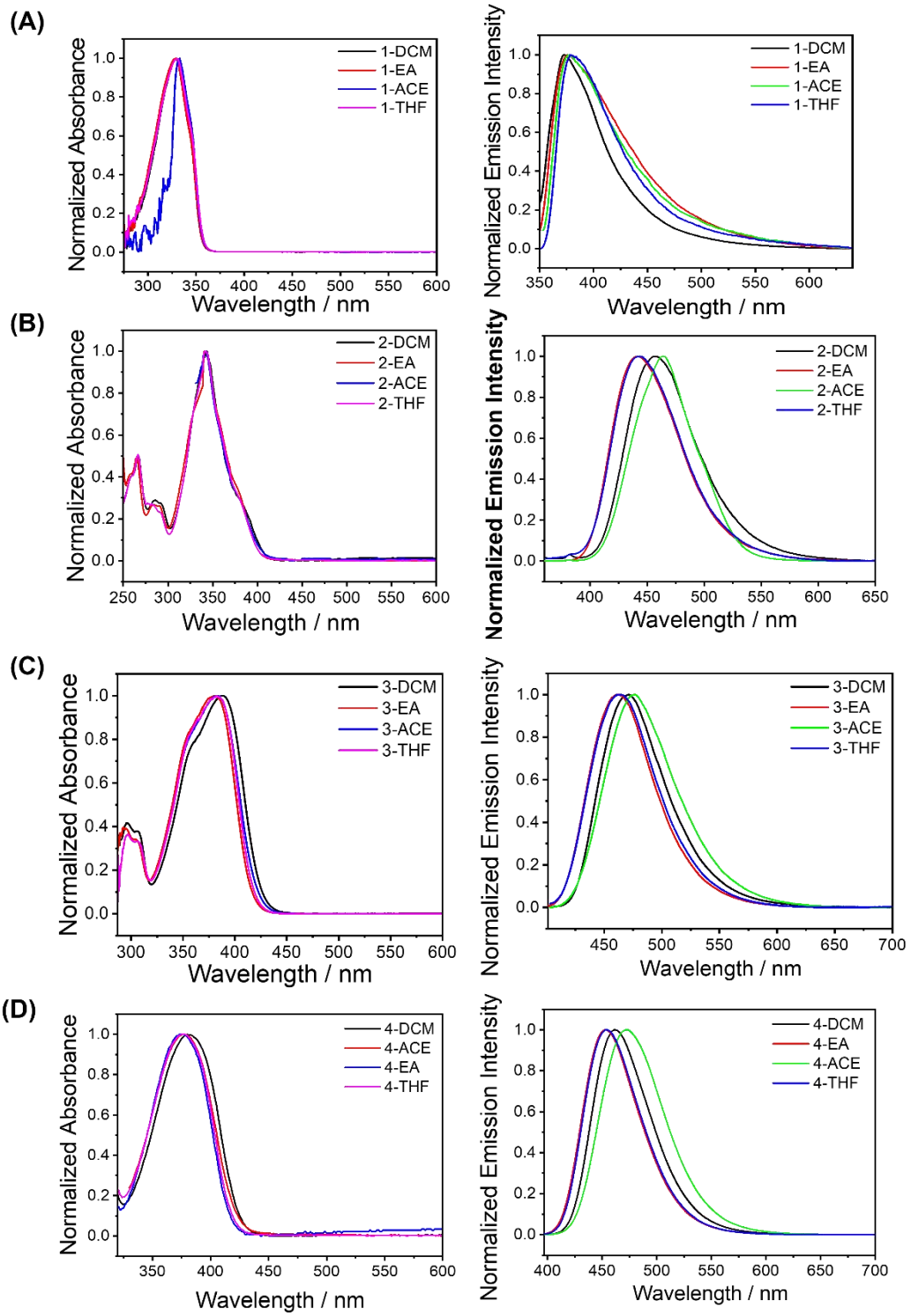

Figure S3. UV-vis absorption spectra and steady-state emission spectra (excited at 365 nm) of **BF_2bdk** in different solvents. DCM, EA, ACE and THF refer to dichloromethane, ethyl acetate, acetone and tetrahydrofuran, respectively.

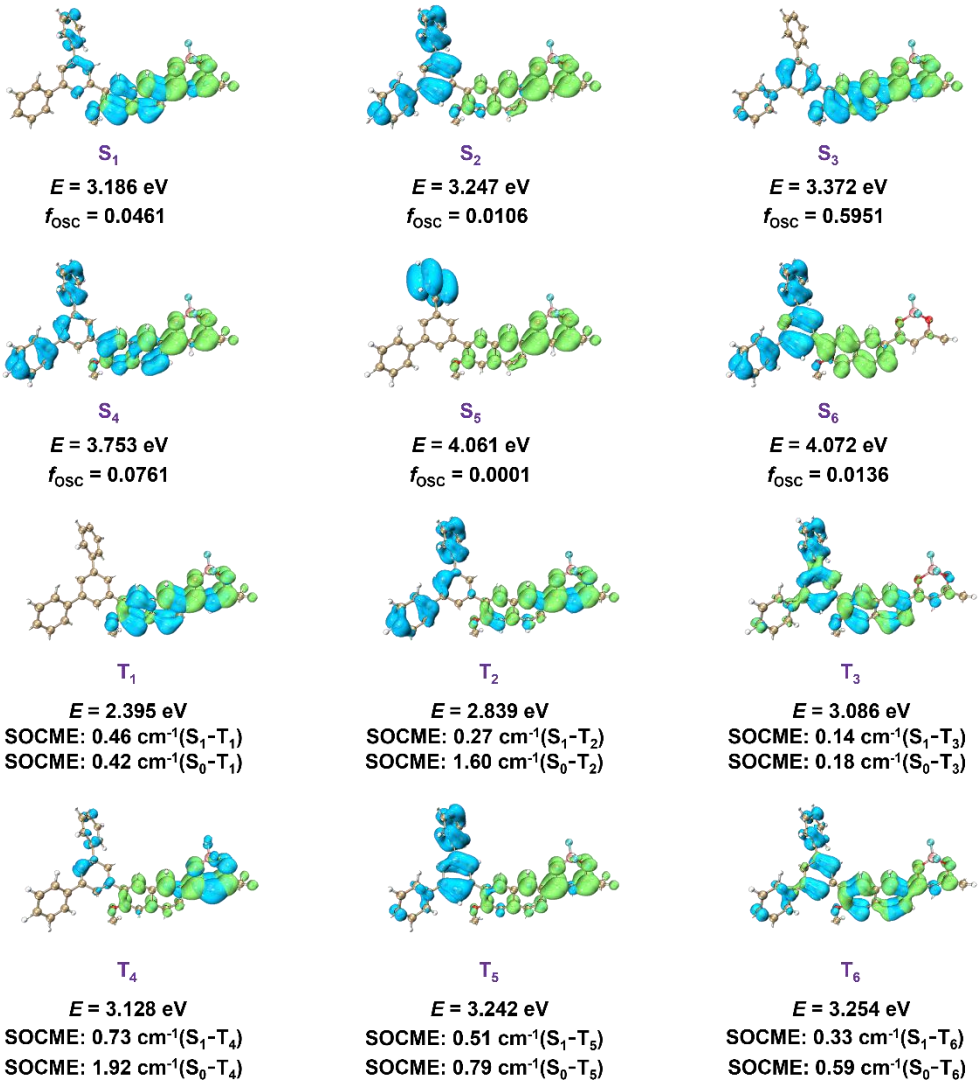

Figure S4. Iso-surface maps of electron-hole density difference of compound **4**'s excited states calculated at B3LYP/def2-TZVP(-f) level, where blue and green iso-surfaces correspond to hole and electron distributions, respectively. TD-DFT calculations show that compound **4** show typical ICT characteristic, and there are several T_n states (such T_1, T_2, T_3) show different excited state nature from S_1 states. According to the El-Sayed rule, such different symmetry between S_1 and T_n states would enhance singlet-to-triplet intersystem crossing. The S_1-to-T_1, S_1-to-T_2 and S_1-to-T_3 ISC channels possess large SOCME of 0.46 cm^{-1}, 0.27 cm^{-1} and 0.14 cm^{-1}, respectively; S_1-to-T_1, S_1-to-T_2 and S_1-to-T_3 ISC channels facilitate the intersystem crossing of compound **4**. The combination of more diverse S_1-T_n channels, moderate SOCME value, stronger S_1 state dipole moments (Table S1) and smaller ΔE_{ST} values (experimental value ~ 0.34 eV) favour the efficient singlet-to-triplet ISC process and the phosphorescence emission of compound **4**. With the assist of PhB matrices, the 0.01%-**4**-PhB materials exhibited RTP mechanim with long emission lifetimes (other afterglow mechanisms have been ruled out in Text S3).

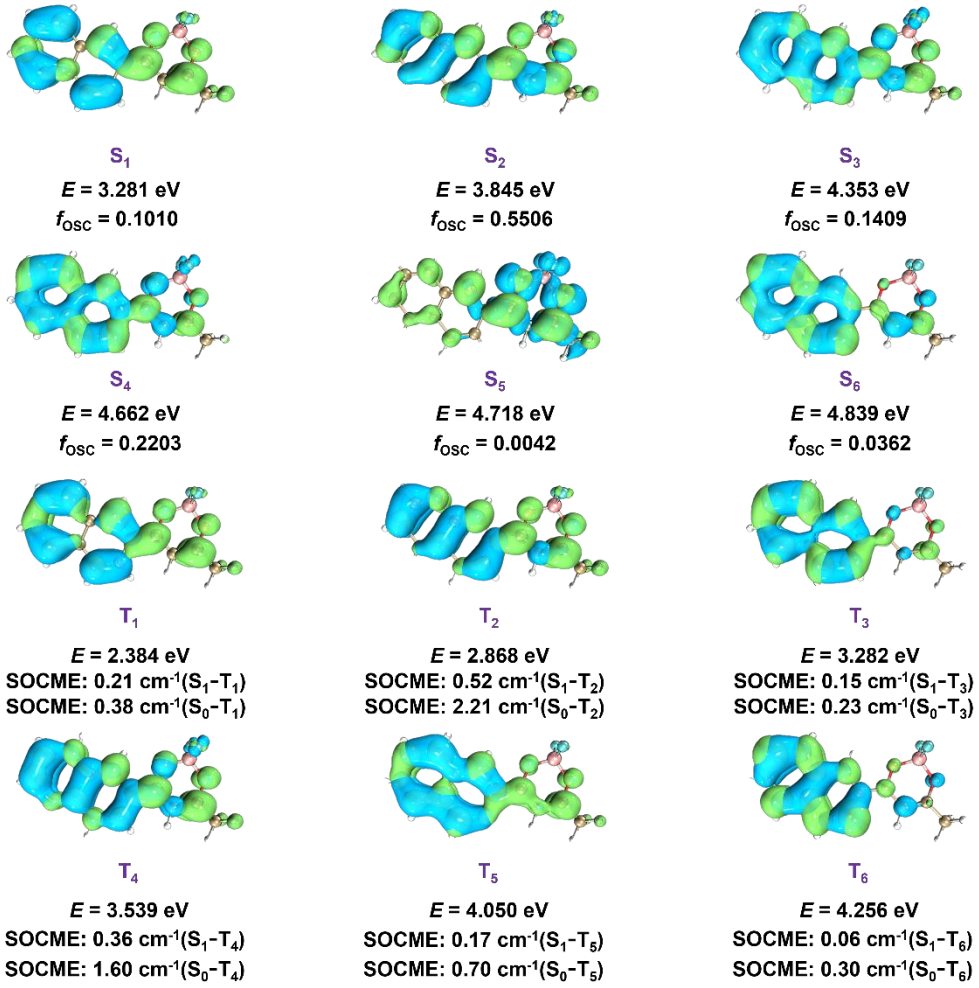

Figure S5. Iso-surface maps of electron-hole density difference of compound **2**'s excited states calculated at B3LYP/def2-TZVP(-f) level, where blue and green iso-surfaces correspond to hole and electron distributions, respectively. TD-DFT calculations show that compound **2** show typical ICT characteristic, and though S_1 and T_1 states of compound **2** show similar excited state symmetry, there are several T_n states (such T_2, T_3) show different excited state nature from S_1 states. According to the El-Sayed rule, such different symmetry between S_1 and T_n states would enhance singlet-to-triplet intersystem crossing. The S_1-to-T_2 and S_1-to-T_3 ISC channels possess relatively small singlet-triplet energy gap with SOCME of 0.52 cm^{-1} and 0.15 cm^{-1} when compared to S_1-to-T_1 ISC channel, and SOCME(sum) = SOCME(S_1-T_1) + SOCME(S_1-T_2) + SOCME(S_1-T_3) = 0.88 cm^{-1}; S_1-to-T_2 and S_1-to-T_3 ISC channels facilitate the intersystem crossing of compound **2**. This is our understanding on the singlet-to-triplet ISC in compound **2** system. With the assist of PhB matrices, the 0.01%-**2**-PhB materials exhibited RTP mechanim with long emission lifetimes (other afterglow mechanisms have been ruled out in Text S3).

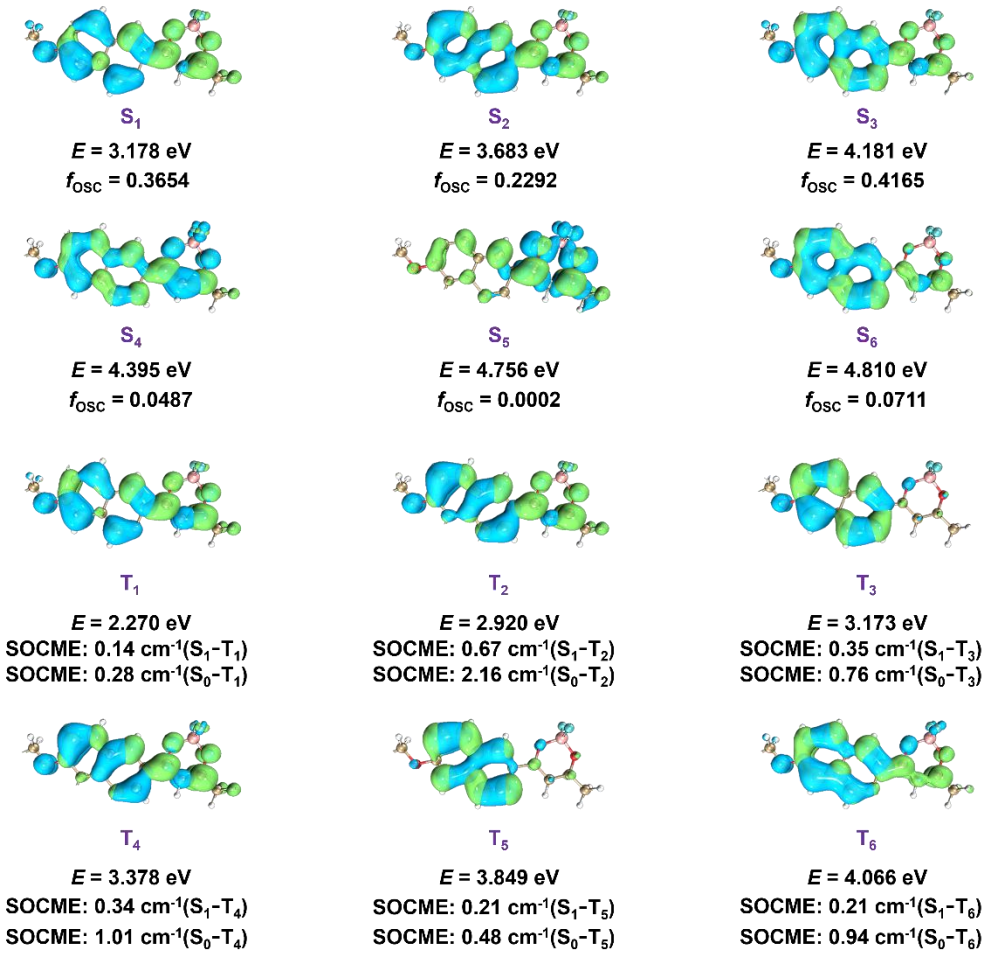

Figure S6. Iso-surface maps of electron-hole density difference of compound **3**'s excited states calculated at B3LYP/def2-TZVP(-f) level, where blue and green iso-surfaces correspond to hole and electron distributions, respectively. TD-DFT calculations show that compound **3** show typical ICT characteristic, and though S_1 and T_1 states of compound **3** show similar excited state symmetry, there are several T_n states (such T_2, T_3) show different excited state nature from S_1 states. According to the El-Sayed rule, such different symmetry between S_1 and T_n states would enhance singlet-to-triplet intersystem crossing. The S_1-to-T_2 and S_1-to-T_3 ISC channels possess relatively small singlet-triplet energy gap with SOCME of 0.67 cm^{-1} and 0.35 cm^{-1} when compared to S_1-to-T_1 ISC channel; S_1-to-T_2 and S_1-to-T_3 ISC channels facilitate the intersystem crossing of compound **3**. SOCME(sum) = SOCME(S_1-T_1) + SOCME(S_1-T_2) + SOCME(S_1-T_3) = 1.16 cm^{-1}; compared to compound **2** (SOCME(sum) = 0.88 cm^{-1}), a significant increase (0.28) in SOCME(sum) occurred for compound **3**, suggesting a notable improvement in its ISC ability. This is our understanding on the singlet-to-triplet ISC in compound **3** system. With the assist of PhB matrices, the 0.01%-**3**-PhB materials exhibited RTP mechanim with long emission lifetimes (other afterglow mechanisms have been ruled out in Text S3).

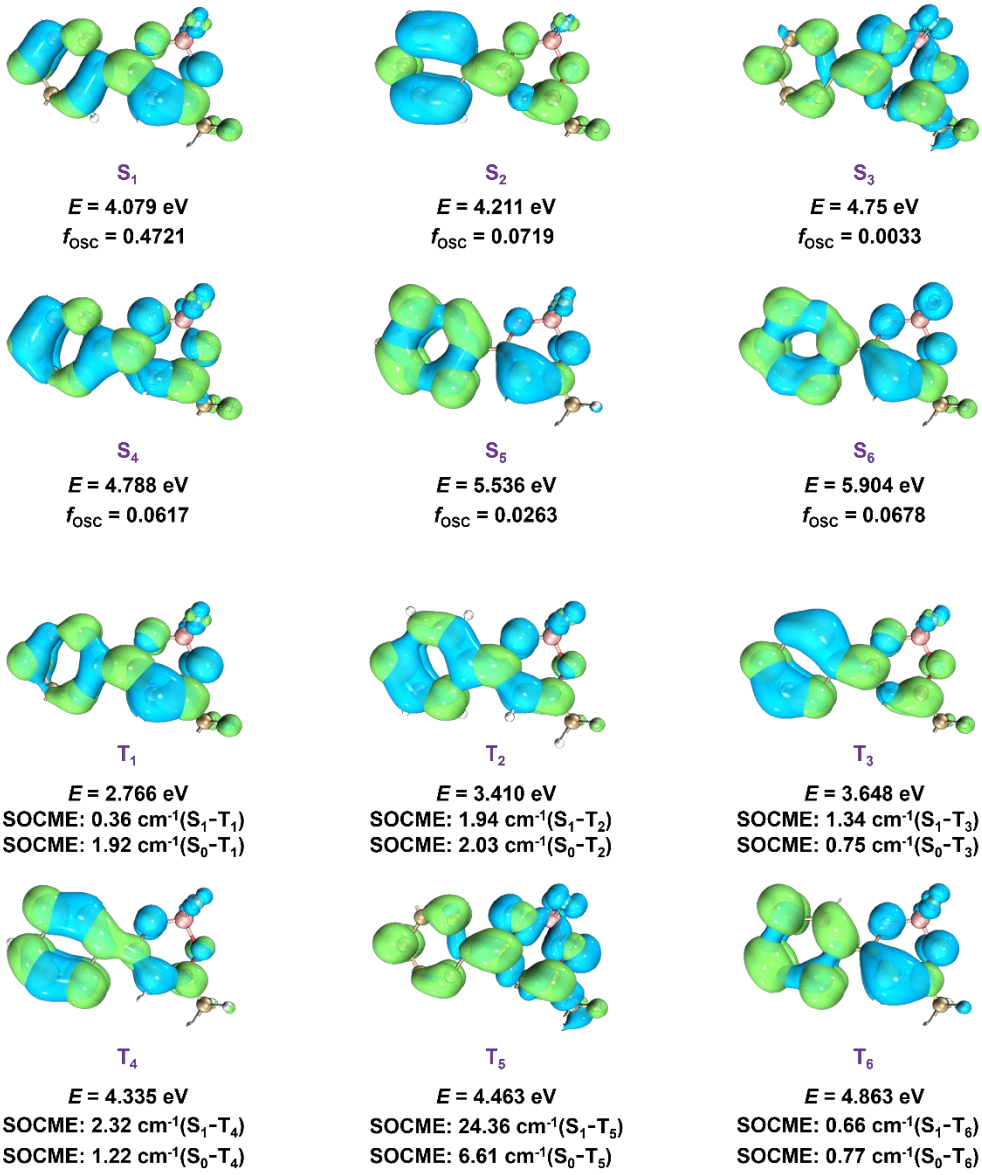

Figure S7. Iso-surface maps of electron-hole density difference of compound **1**'s excited states calculated at B3LYP/def2-TZVP(-f) level, where blue and green iso-surfaces correspond to hole and electron distributions, respectively. TD-DFT calculations show that both S_1 and T_1 states of compound **1** show similar LE characteristic, which are unfavourable for intersystem crossing process. This is also consistent with the experimental observation that **1**-PhB show insignificant fluorescence and phosphorescence at room temperature.

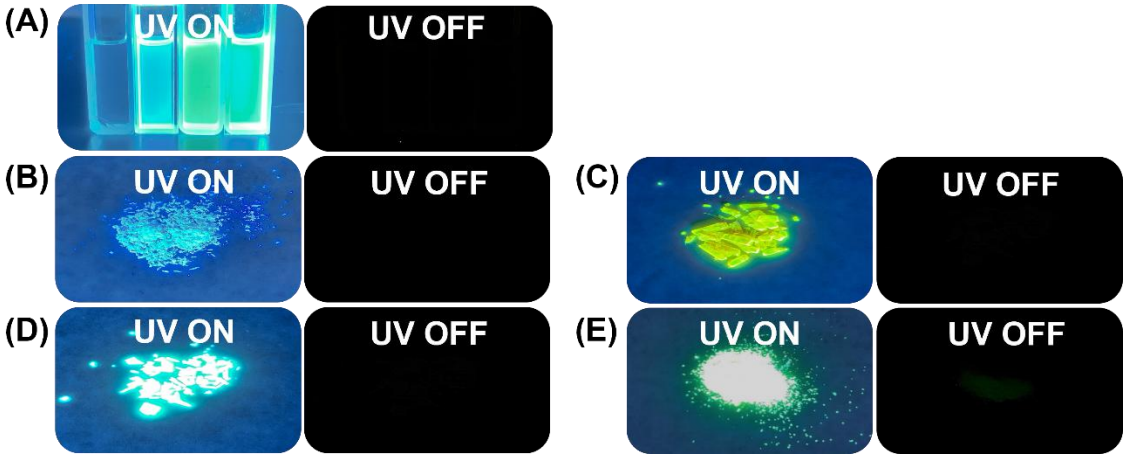

Figure S8. (A) Photographs of **BF_2bdk** molecules in dichloromethane solution under 365 nm UV light and after removal of UV light. (B-E) Photographs of compounds **1**, **2**, **3**, and **4** in the solid state under 365 nm UV light and after removal of UV light.

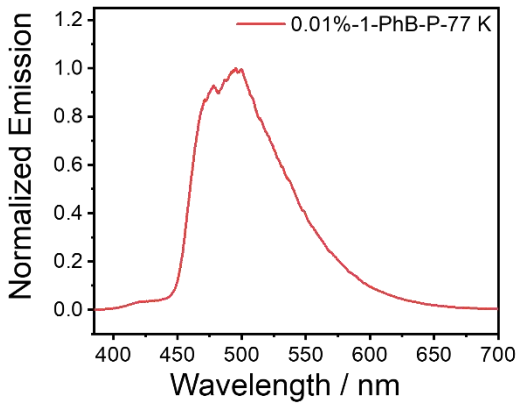

Figure S9. The steady-state and delayed emission spectra of **1**-PhB sample (excited at 365 nm) at 77 K.

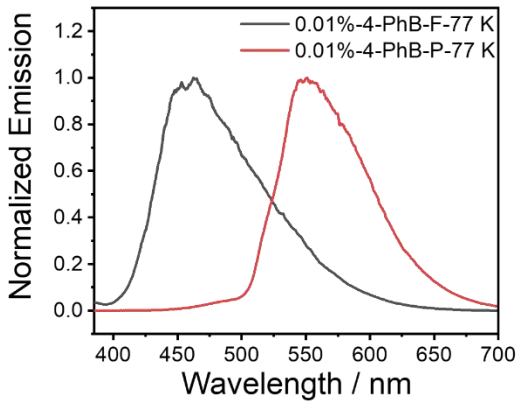

Figure S10. Steady-state and delayed emission spectra of **4**-PhB (excited at 365 nm) at 77 K.

Table S2. Calculation results of dipole moments of **BF_2bdk**'s S_1 states.

Compounds	**1**	**2**	**3**	**4**
Dipole moment / Debye	8.40	20.18	23.10	24.78

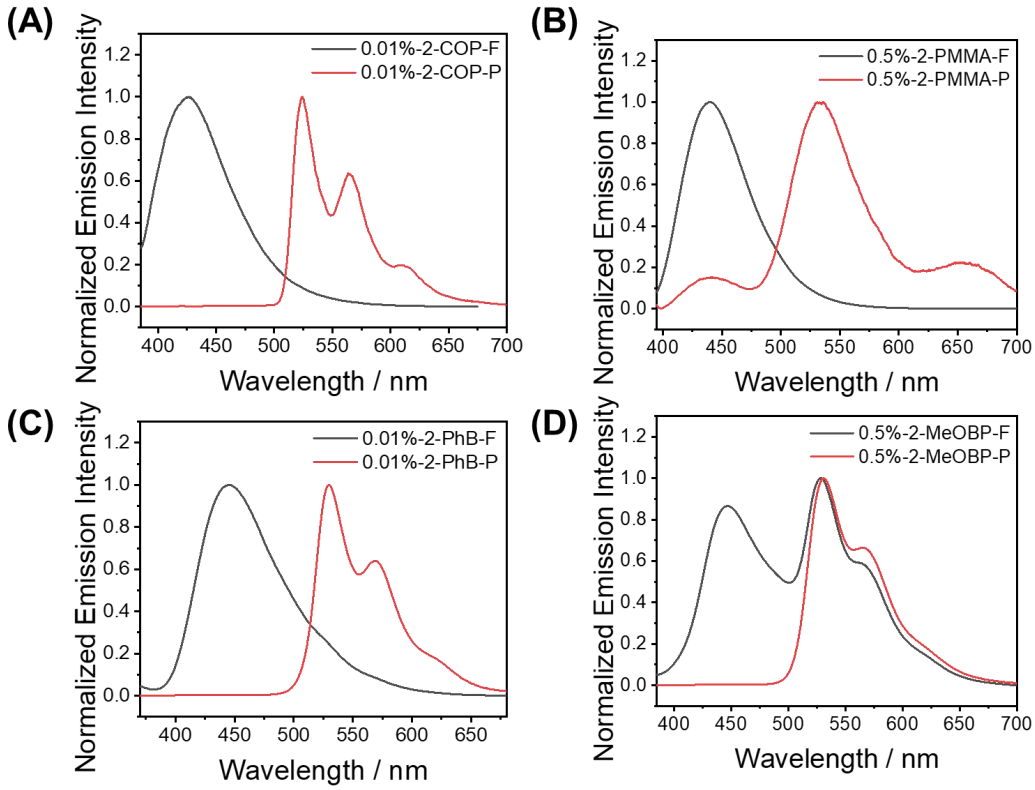

Figure S11. (A) The room-temperature steady-state and delayed emission spectra (1 ms delay, 77 K) of **2**-COP sample excited at 365 nm. (B-D) The room-temperature steady-state and delayed emission spectra (1 ms delay) of other **2**-matrix samples excited at 365 nm. COP, PMMA, PhB and MeOBP refer to cyclo olefin polymer, poly(methyl methacrylate), phenyl benzoate and 4-methoxybenzophenone, respectively.

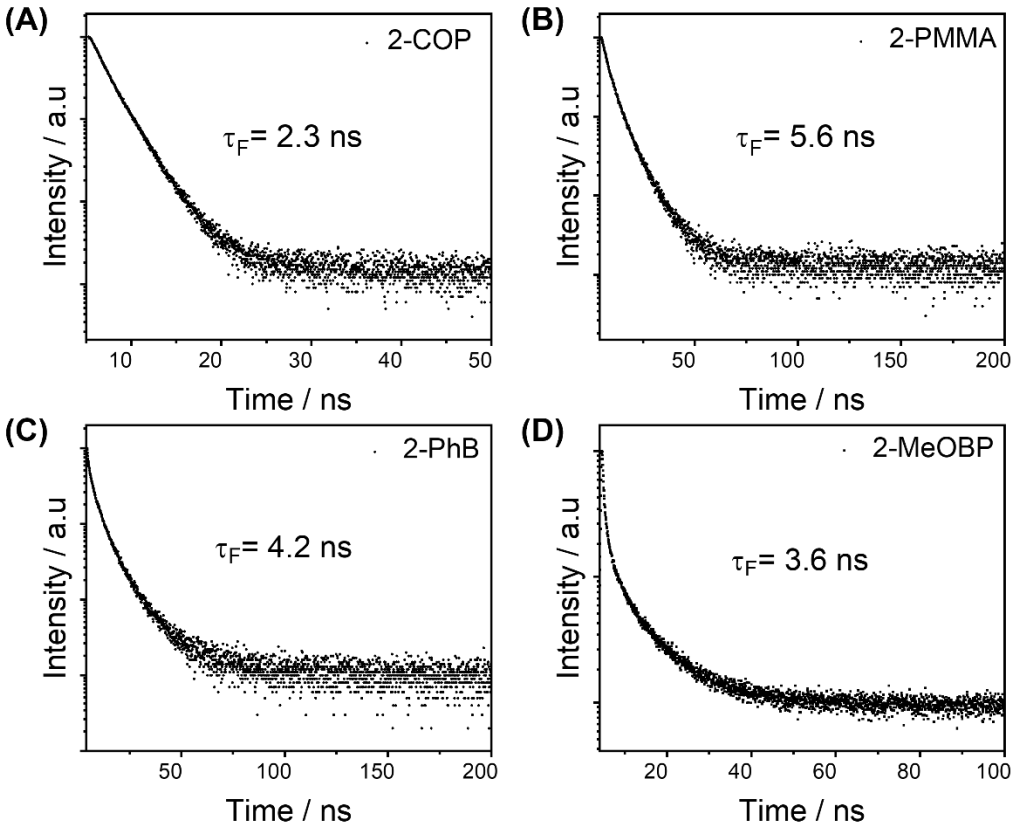

Figure S12. The fluorescence decay profiles of **2**-matrix samples (excited at 365 nm) at room temperature.

Table S3. Photophysical property of **2**-matrix samples.

Entry	λ_F / nm	τ_F / ns	τ_{AVG} / ns	λ_P / nm	ΔE_{ST} / eV
2-COP	391	τ_1 = 1.73 ns (57.4%) τ_2 = 2.87 ns (42.6%)	2.3	525	0.809
2-PMMA	440	τ_1 = 3.12 ns (48.6%) τ_2 = 8.25 ns (51.4%)	5.8	535	0.500
2-PhB	442	τ_1 = 0.48 ns (6.2%) τ_2 = 3.84 ns (58.8%) τ_3 = 10.94 ns (35.0%)	6.1	529	0.461
2-MeOBP	447	τ_1 = 0.35 ns (18.7%) τ_2 = 2.04 ns (27.0%) τ_3 = 9.34 ns (54.3%)	3.6	530	0.434

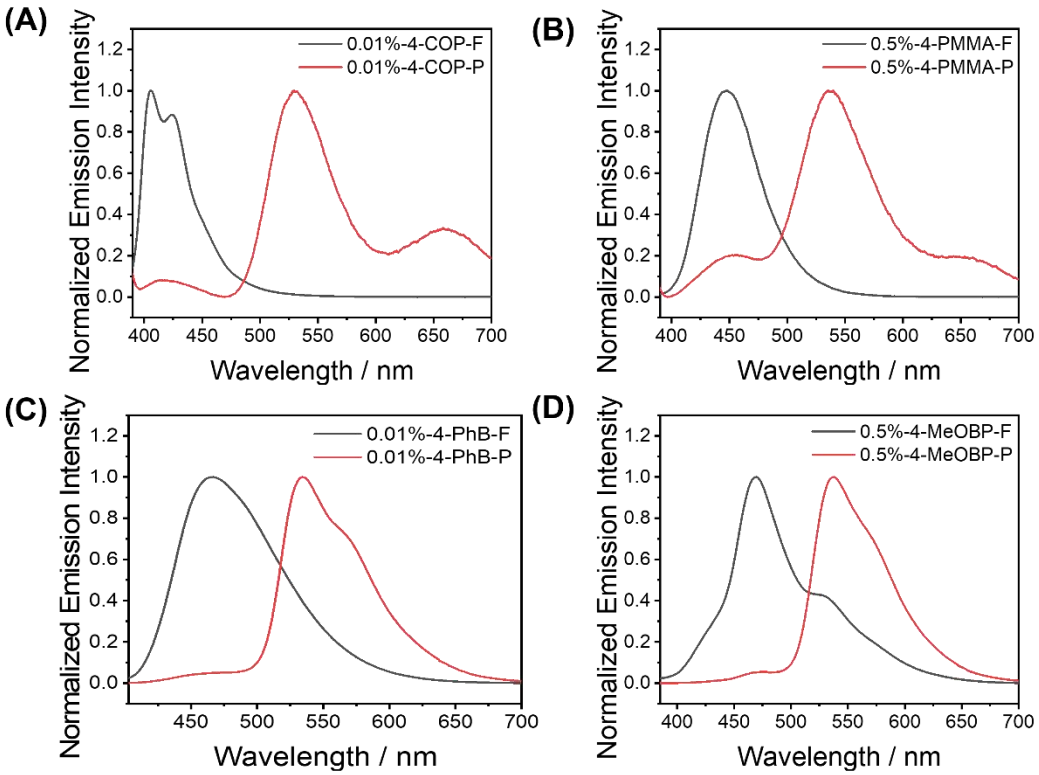

Figure S13. The steady-state and delayed emission spectra of **4**-matrix samples (excited at 365 nm) at room temperature.

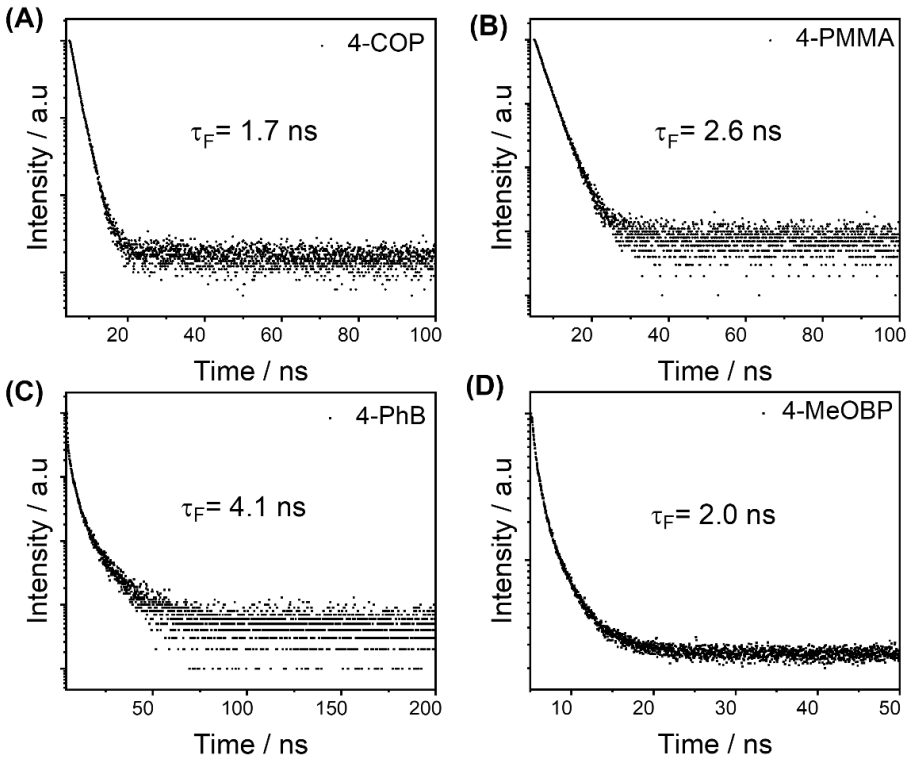

Figure S14. The fluorescence decay profiles of **4**-matrix samples (excited at 365 nm) at room temperature.

Table S4. Photophysical property of **4**-matrix samples.

Entry	λ_F / nm	τ_F / ns	τ_{AVG} / ns	λ_P / nm	ΔE_{ST} / eV
4-COP	405	τ_1 = 0.08 ns (88.9%) τ_2 = 1.92 ns (11.1%)	1.7	531	0.727
4-PMMA	448	τ_1 = 2.18 ns (72.5%) τ_2 = 3.43 ns (27.5%)	2.6	534	0.446
4-PhB	467	τ_1 = 0.34 ns (23.0%) τ_2 = 0.64 ns (53.4%) τ_3 = 10.97 ns (23.7%)	4.1	534	0.333
4-MeOBP	470	τ_1 = 0.61 ns (35.8%) τ_2 = 2.70 ns (64.2%)	2.0	537	0.329

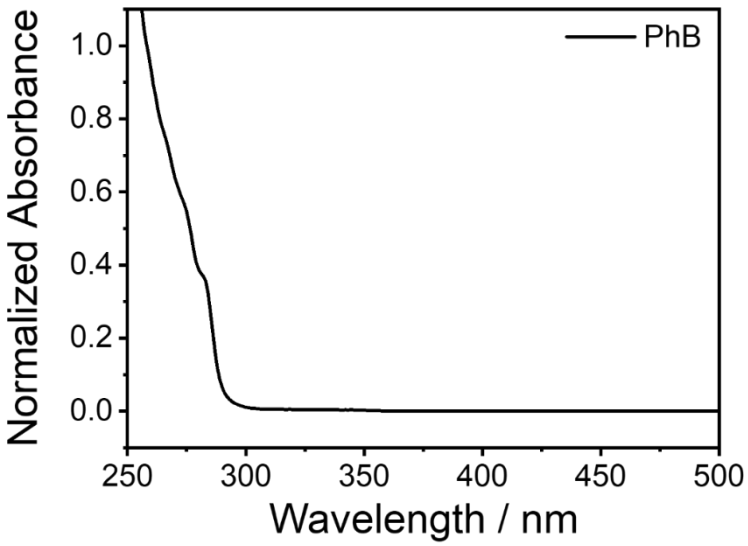

Figure S15. The UV-vis absorption of PhB matrix.

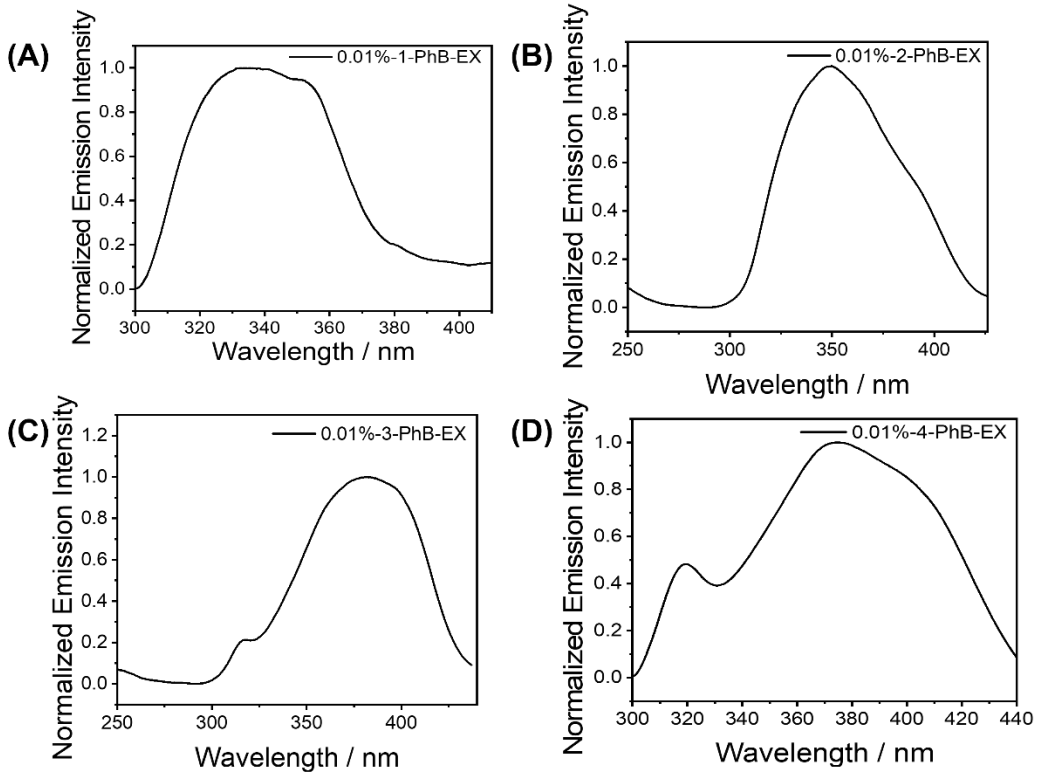

Figure S16. The excitation spectra of **BF_2bdk**-PhB samples.

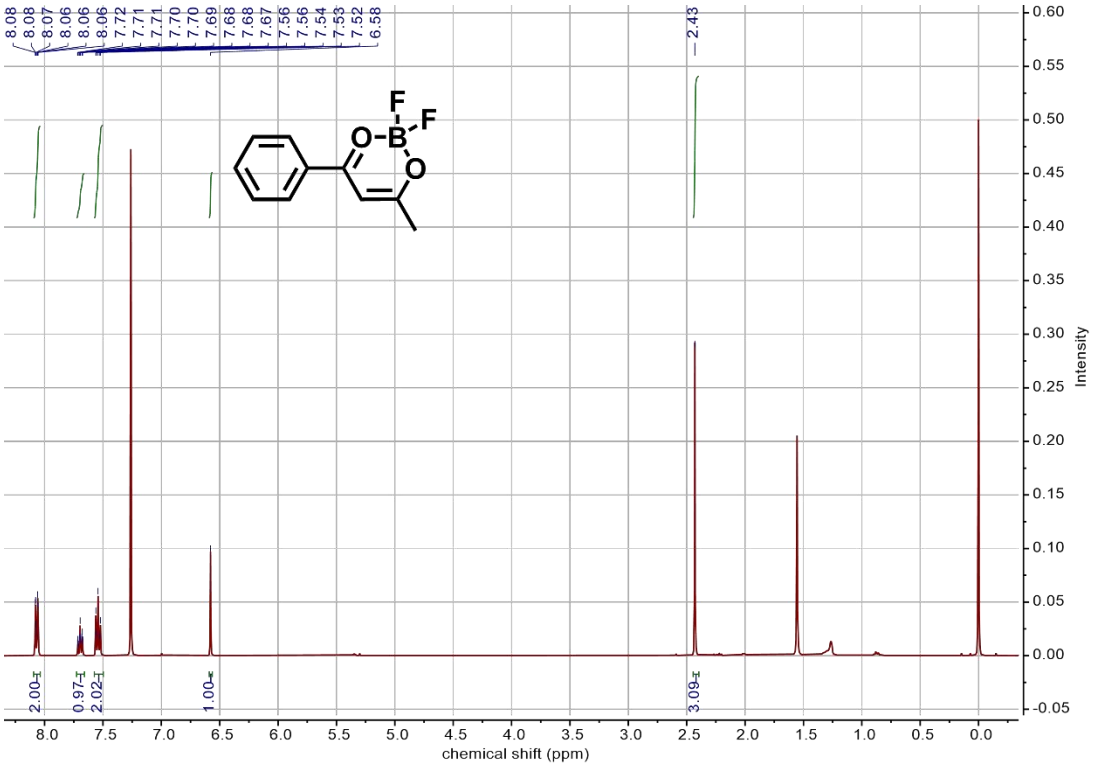

Figure S17. ^{1}H NMR spectrum of compound **1.**

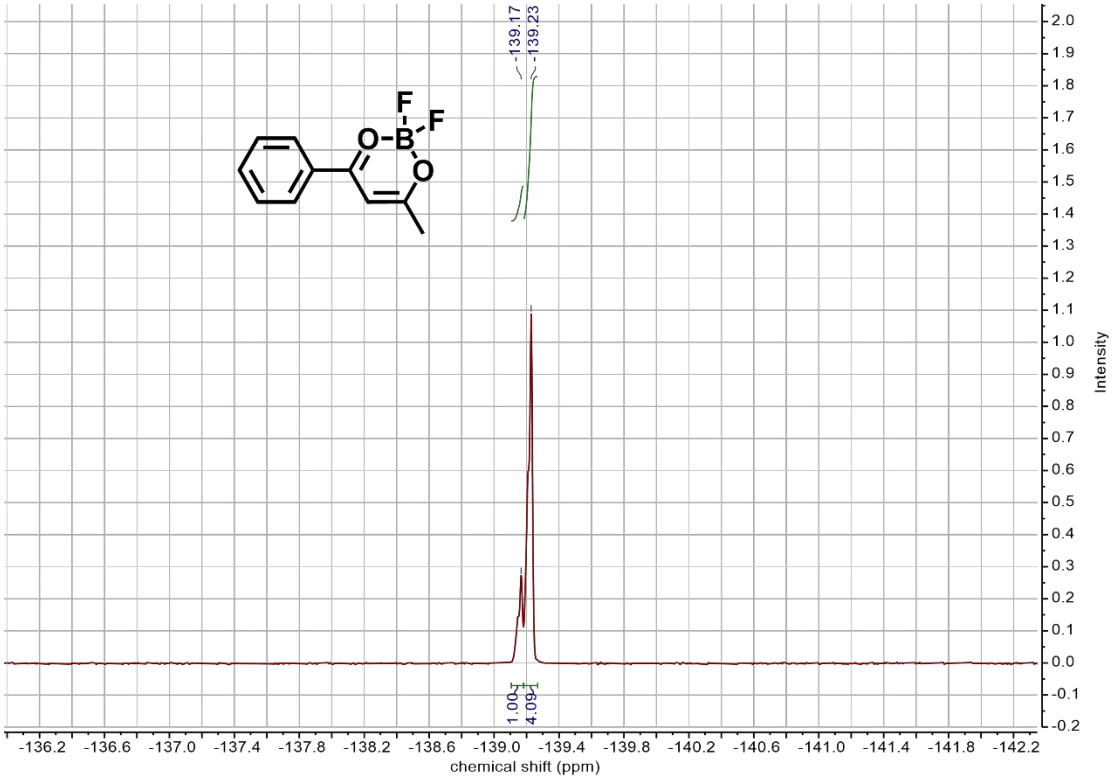

Figure S18. ^{19}F NMR spectrum of compound **1.**

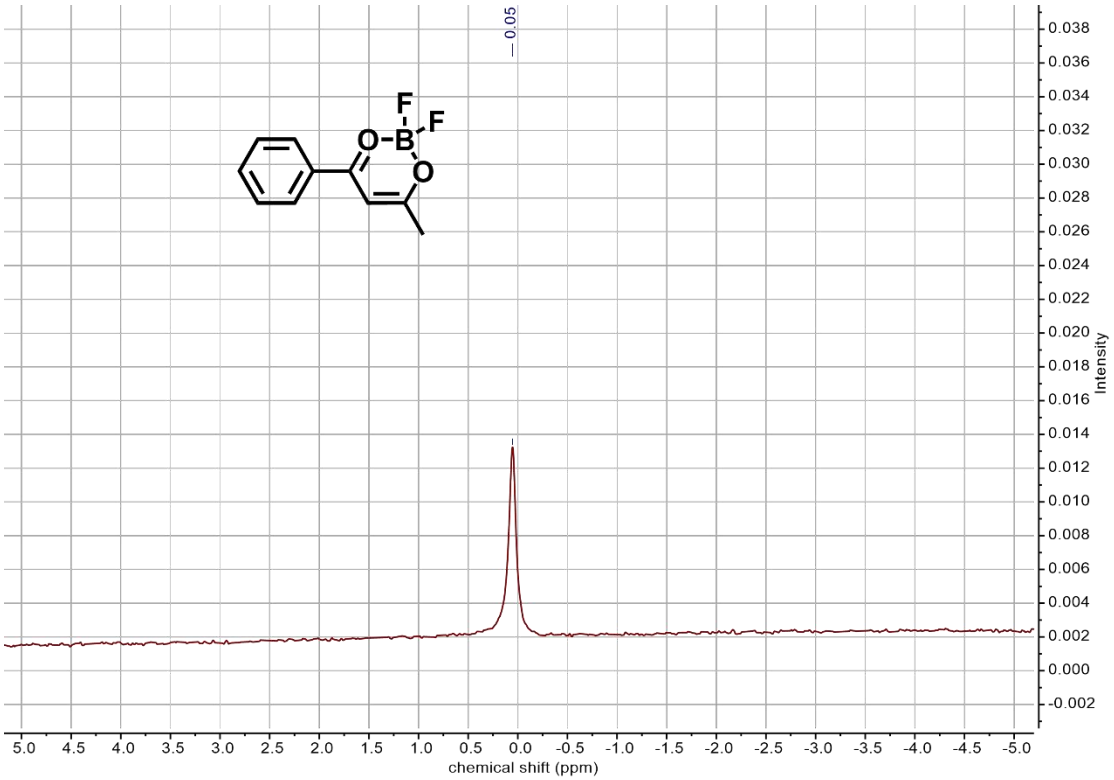

Figure S19. ^{11}B NMR spectrum of compound **1.**

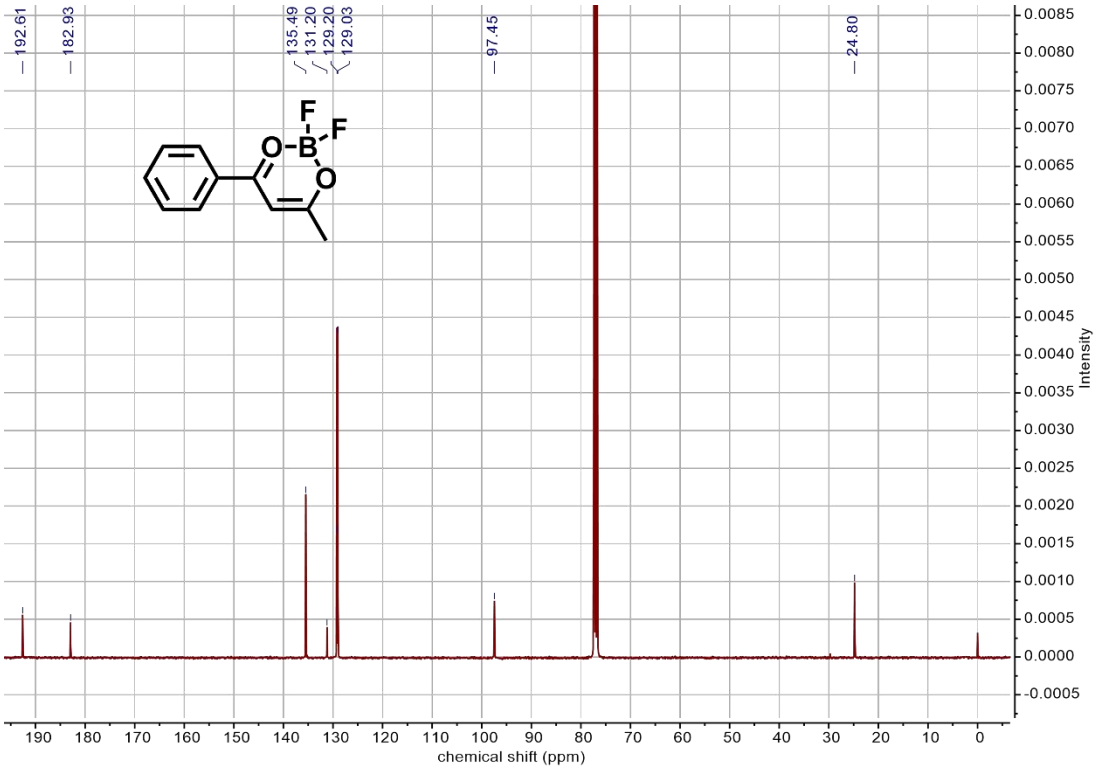

Figure S20. ^{13}C NMR spectrum of compound **1.**

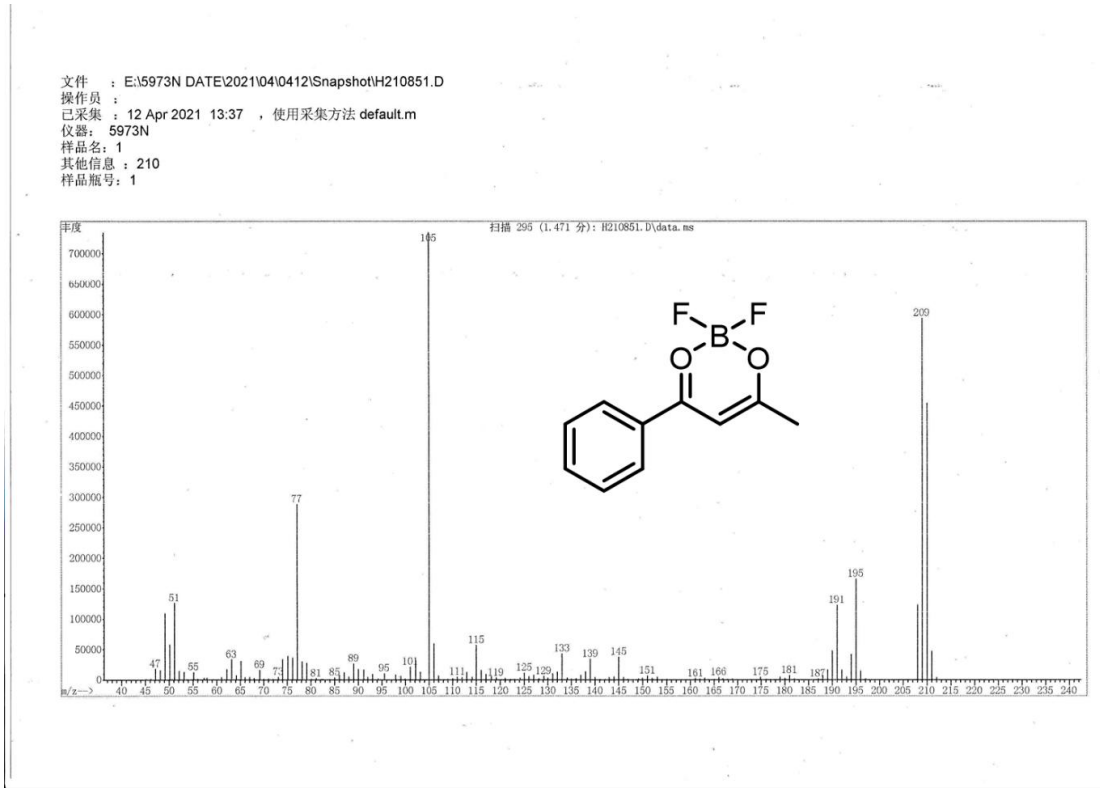

Figure S21. LRMS spectrum of compound **1.**

National Center for Organic Mass Spectrometry in Shanghai
Shanghai Institute of Organic Chemistry
Chinese Academic of Sciences
High Resolution FI-MS Report
Low Resolution FI-MS Report

Instrument: JEOL-AccuTOF-GCv4G-GCT MS

Operation Mode: FI Positive Ion Mode (Counter Electrode: 10000V)

Card Serial Number: GCT-FI-T21-04-1487

Sample Serial Number: 2020274-1

Operator: Li Date: 2021/04/18

m/z	Theo. Mass	Delta (ppm)	RDB equiv.	Composition
209.0690	209.0694	-2.15	6.0	$C_{10}H_9O_2{}^{10}BF_2$
	209.0696	-3.05	3.5	$C_8H_9N_2F_4$
	209.0683	3.32	10.0	$C_{13}H_8O{}^{10}BF$
	209.0683	3.54	6.0	$C_{10}H_{11}O_4N$
	209.0681	4.30	-5.0	$C_2H_{12}O_4NF_5$

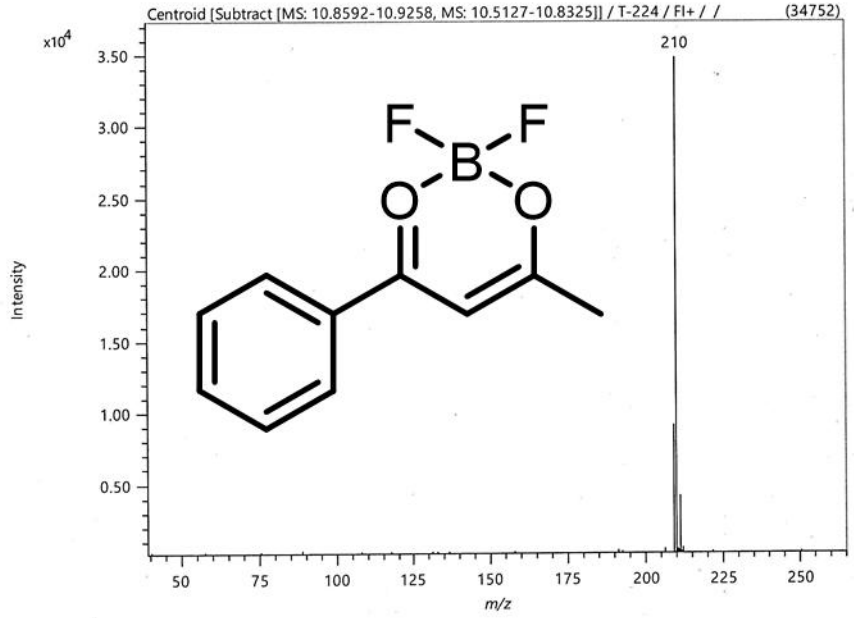

Figure S22. HRMS spectrum of compound **1.**

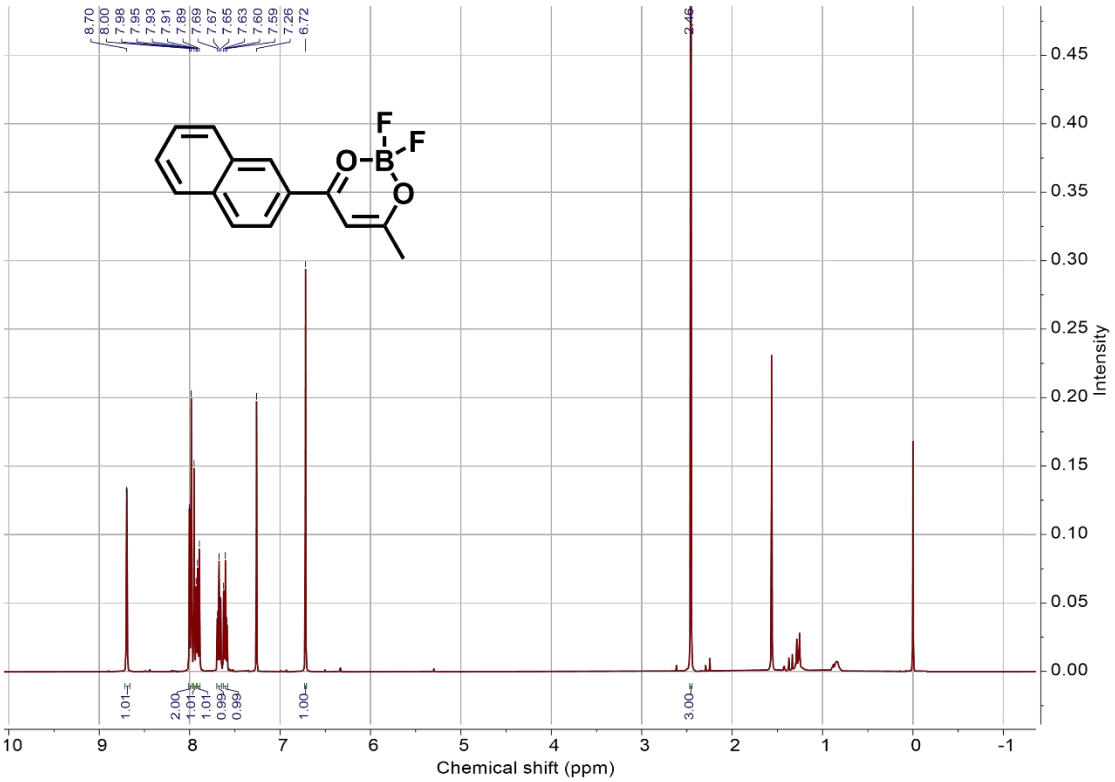

Figure S23. [1]H NMR spectrum of compound **2.**

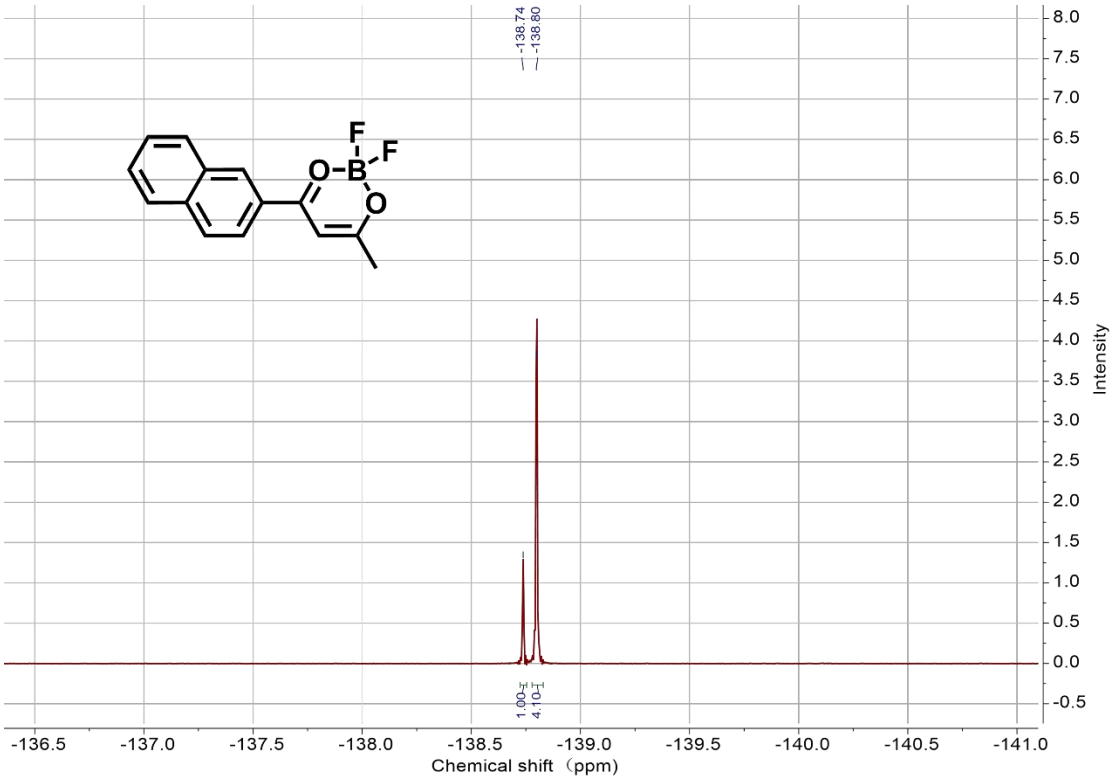

Figure S24. [19]F NMR spectrum of compound **2.**

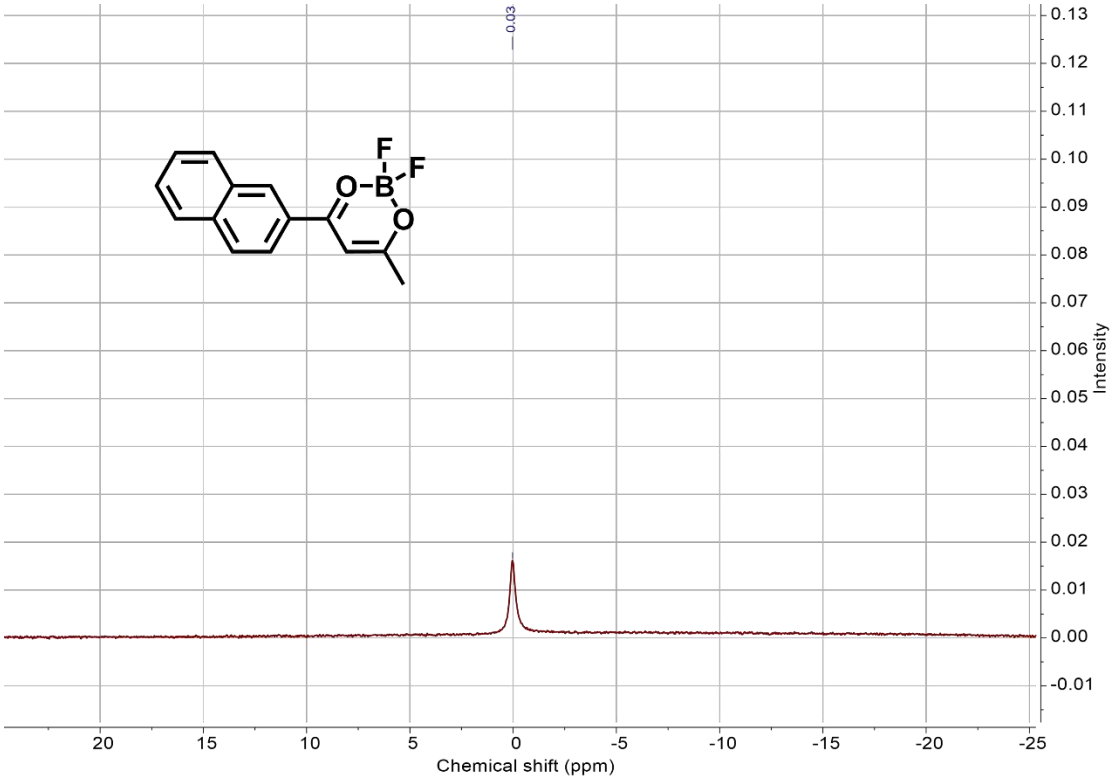

Figure S25. ^{11}B NMR spectrum of compound **2.**

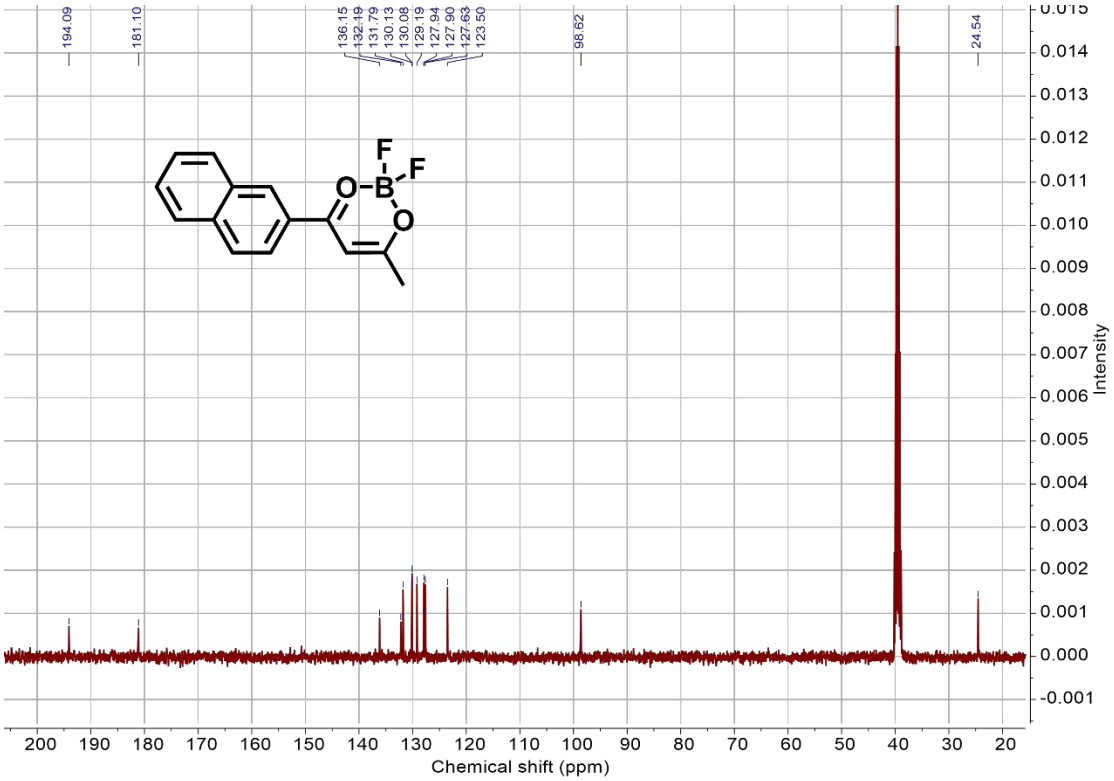

Figure S26. ^{13}C NMR spectrum of compound **2.**

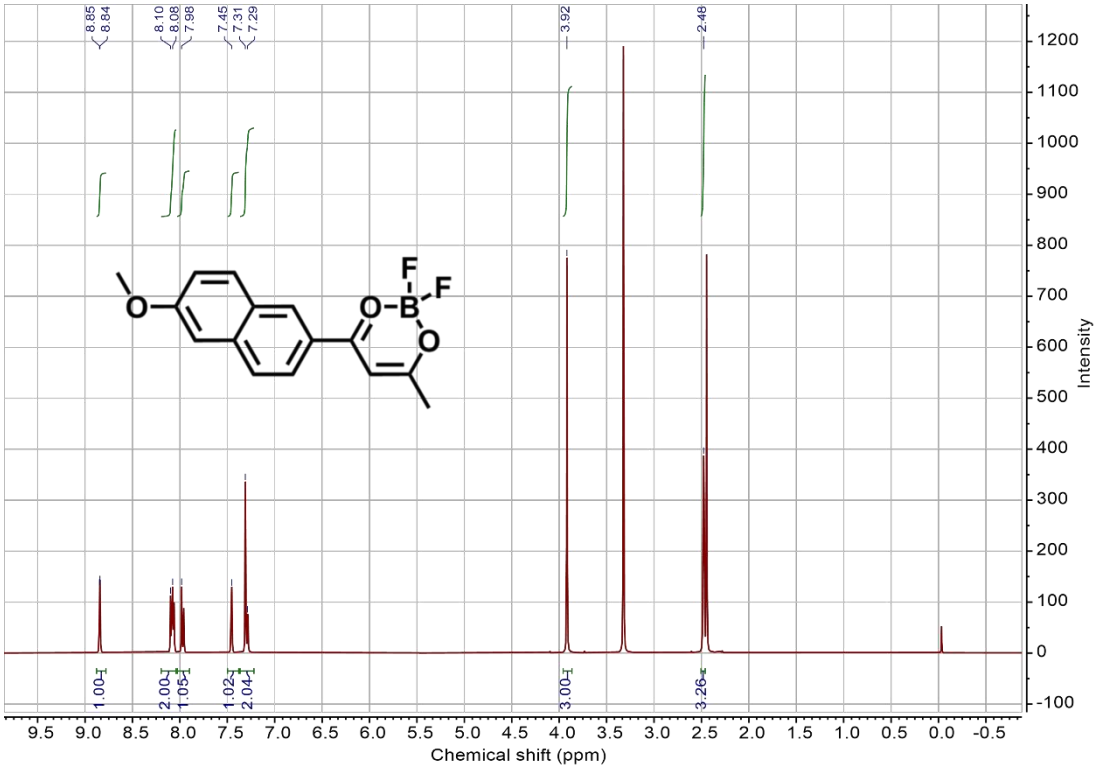

Figure S27. [1]H NMR spectrum of compound **3.**

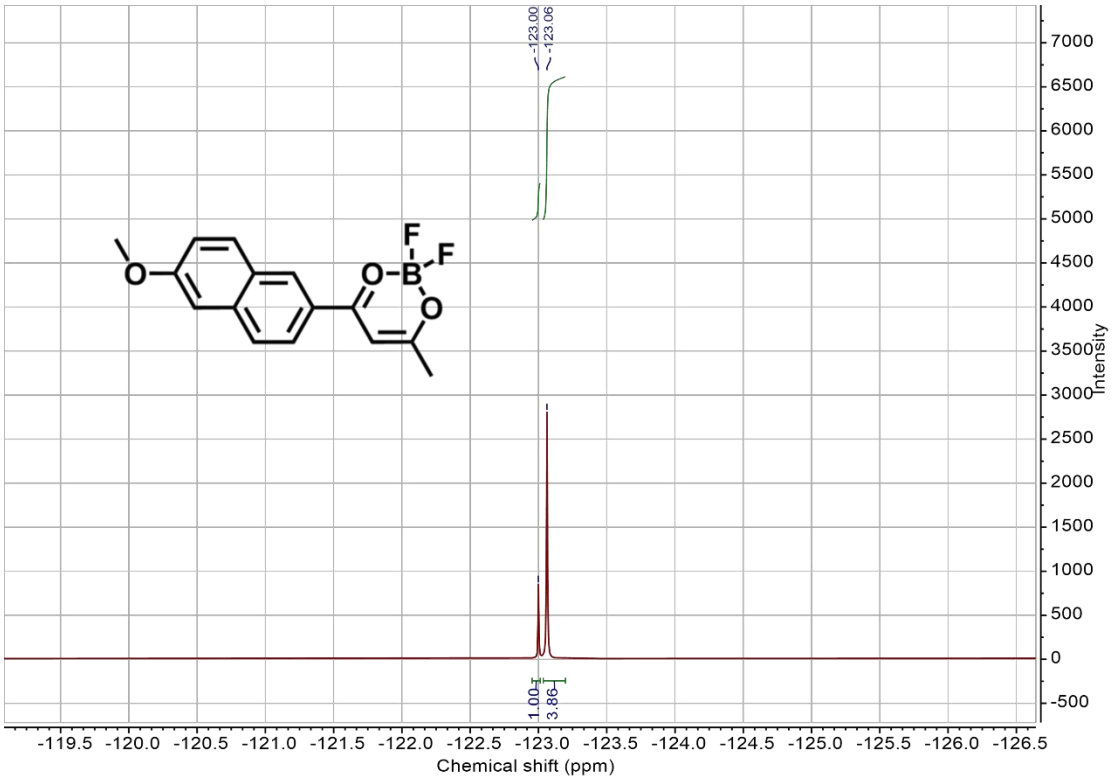

Figure S28. [19]F NMR spectrum of compound **3.**

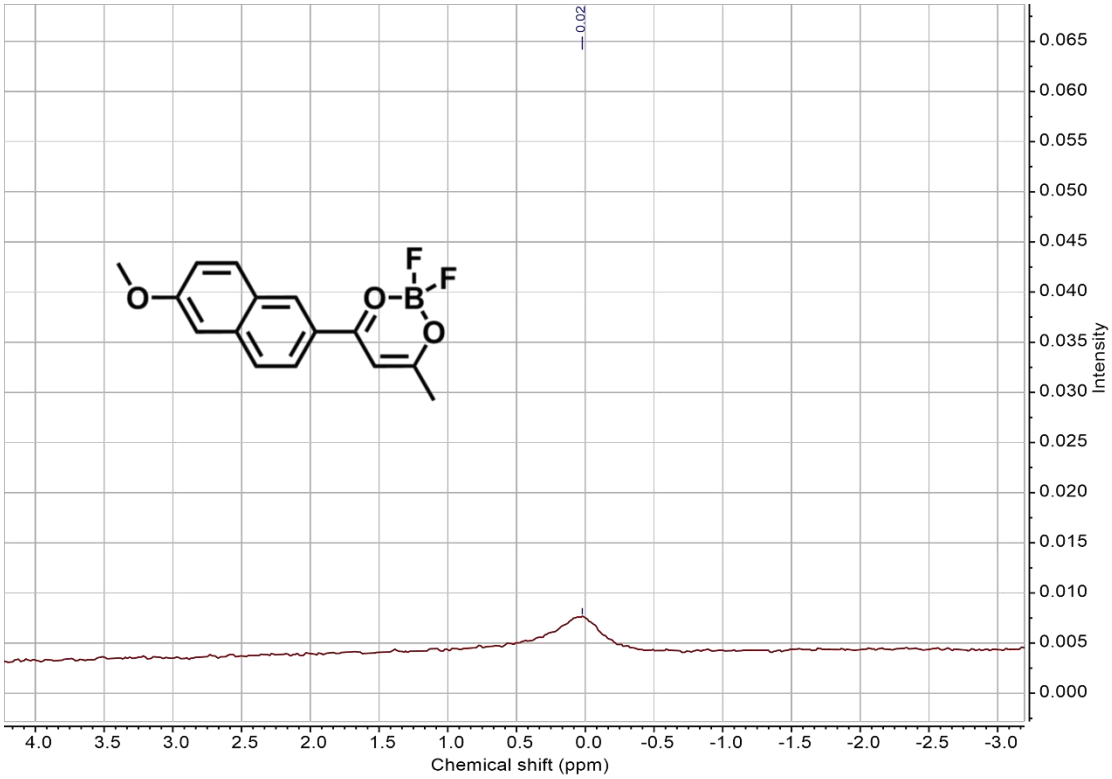

Figure S29. ^{11}B NMR spectrum of compound **3.**

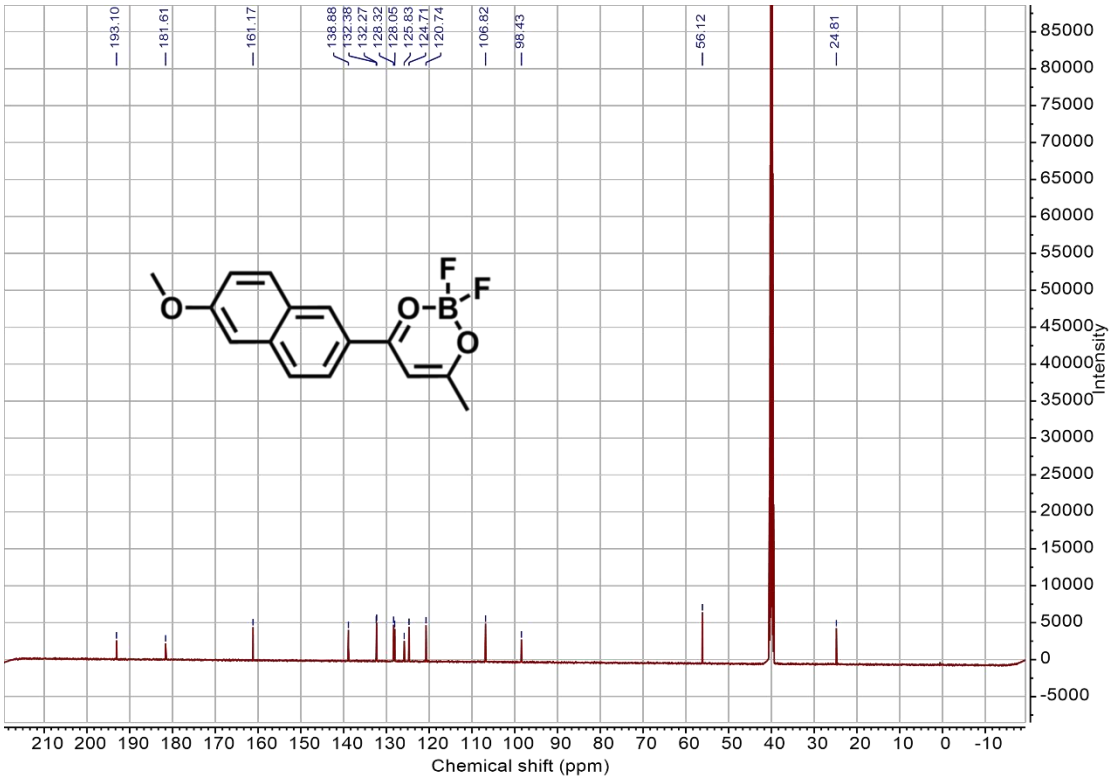

Figure S30. ^{13}C NMR spectrum of compound **3.**

Qualitative Analysis Report

Data Filename	2019115-LX-6.d	**Sample Name**	LX-6
Sample Type	Sample	**Position**	Vial 66
Instrument Name	Instrument 1	**User Name**	
Acq Method	IDJ4-75V.m	**Acquired Time**	10/18/2023 3:26:24 PM
IRM Calibration Status	Success	**DA Method**	FGFUS-C18.m
Comment			
Sample Group		**Info.**	
Acquisition SW Version	6200 series TOF/6500 series Q-TOF B.05.01 (B5125.3)		

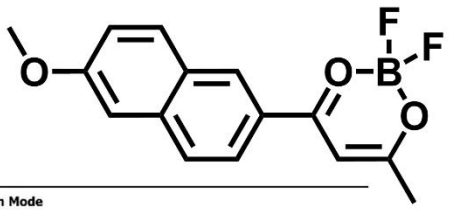

User Spectra

Fragmentor Voltage	Collision Energy	Ionization Mode
175	0	ESI

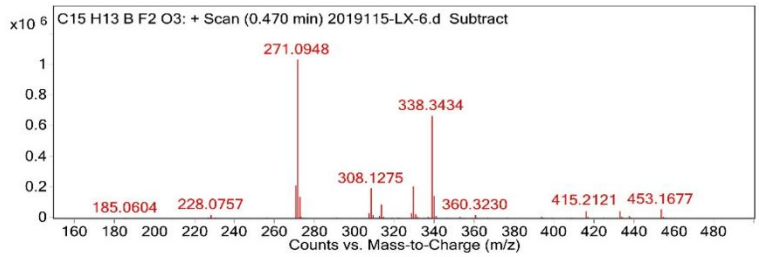

Peak List

m/z	z	Abund	Formula	Ion
307.1300	1	36077.88	C15 H13 B F2 O3	(M+NH4)+
308.1275	1	195997.66	C15 H13 B F2 O3	(M+NH4)+
309.1295	1	25142.82	C15 H13 B F2 O3	(M+NH4)+
312.0851	1	16467.18	C15 H13 B F2 O3	(M+Na)+
313.0825	1	90792.68	C15 H13 B F2 O3	(M+Na)+
314.0848	1	11093.71	C15 H13 B F2 O3	(M+Na)+

Formula Calculator Element Limits

Element	Min	Max
C	3	70
H	0	120
O	1	6
F	1	3
B	1	1

Formula Calculator Results

Ion Formula	m/z	m/z (Calc)	DBE	Diff (ppm)	Score (MFG)
C18 H16 B F N O2	307.1300	307.1289	13	-3.82	95.76
C15 H17 B F2 N O3	307.1300	307.1300	9	0.13	99.99
C18 H12 B F Na O2	312.0851	312.0843	13	-2.8	97.68
C15 H13 B F2 Na O3	312.0851	312.0854	9	1.15	99.6

--- End Of Report ---

Agilent Technologies Page 1 of 1 Printed at: 4:57 PM on: 10/18/2023

Figure S31. HRMS of compound **3.**

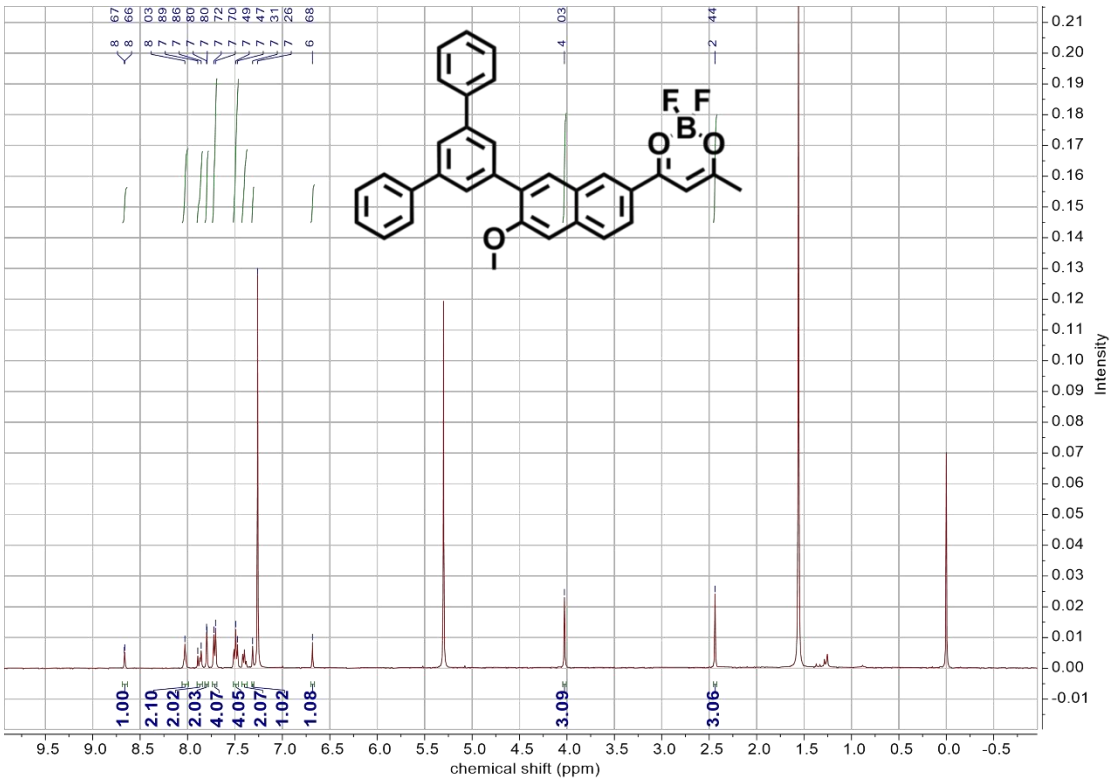

Figure S32. ^{1}H NMR spectrum of compound **4.**

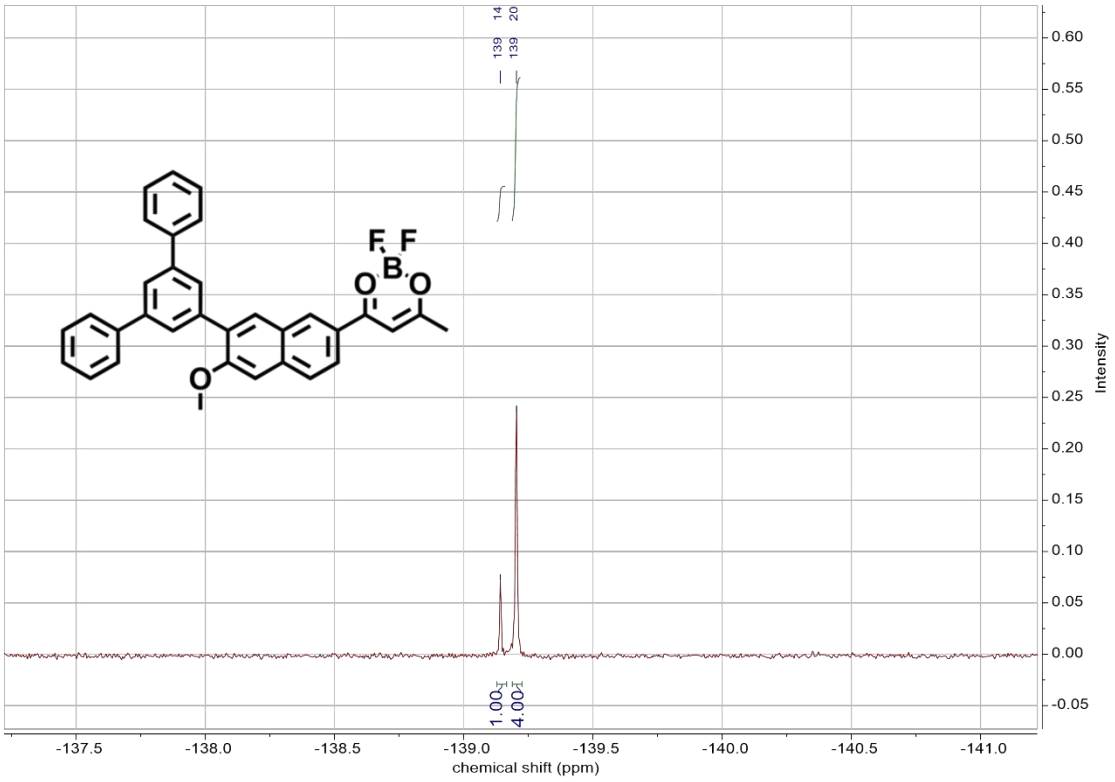

Figure S33. ^{19}F NMR spectrum of compound **4.**

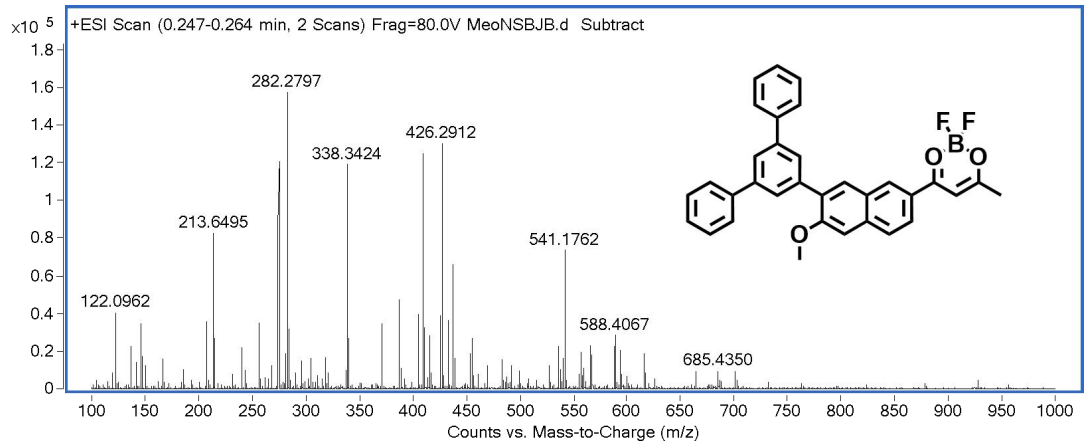

Figure S34. HRMS spectrum of compound **4.**

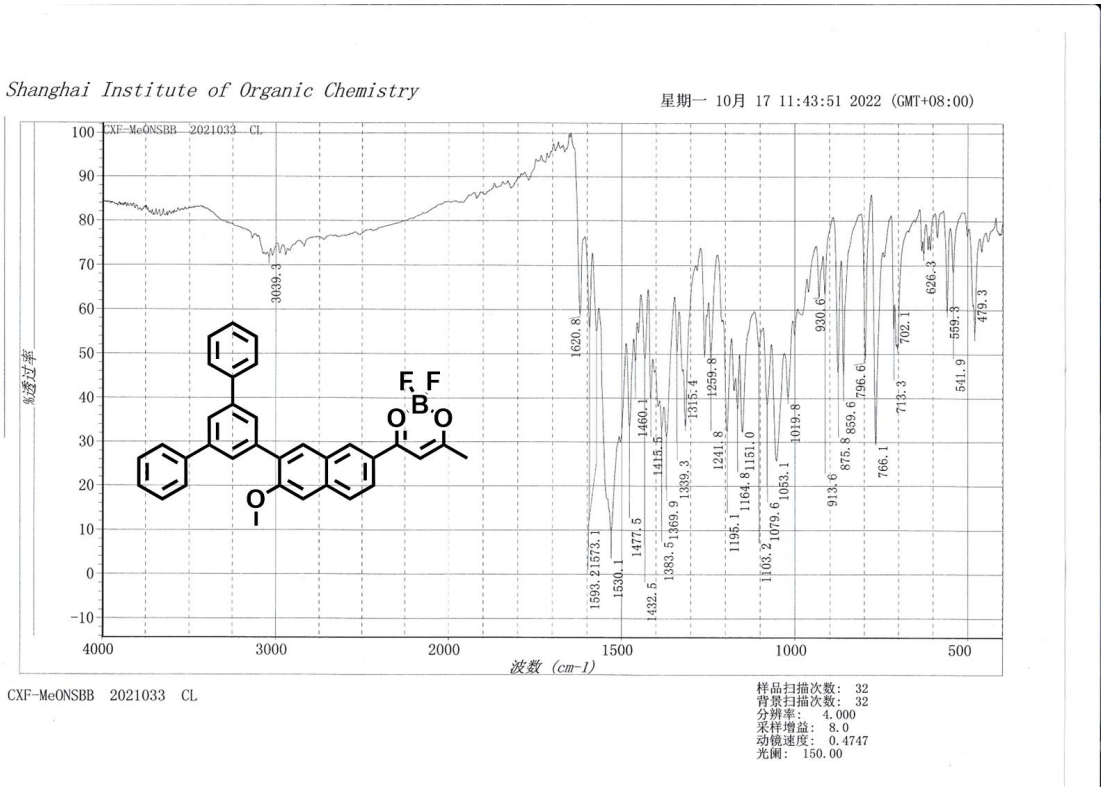

Figure S35. FT-IR spectrum of compound **4.**

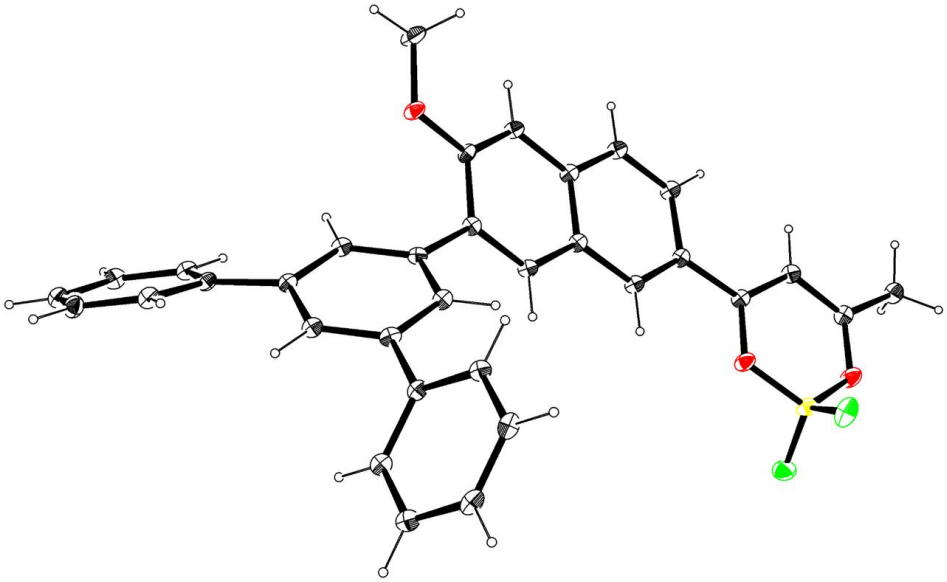

Figure S36. Single crystal structure of compound **4** (CCDC number, 2226200).